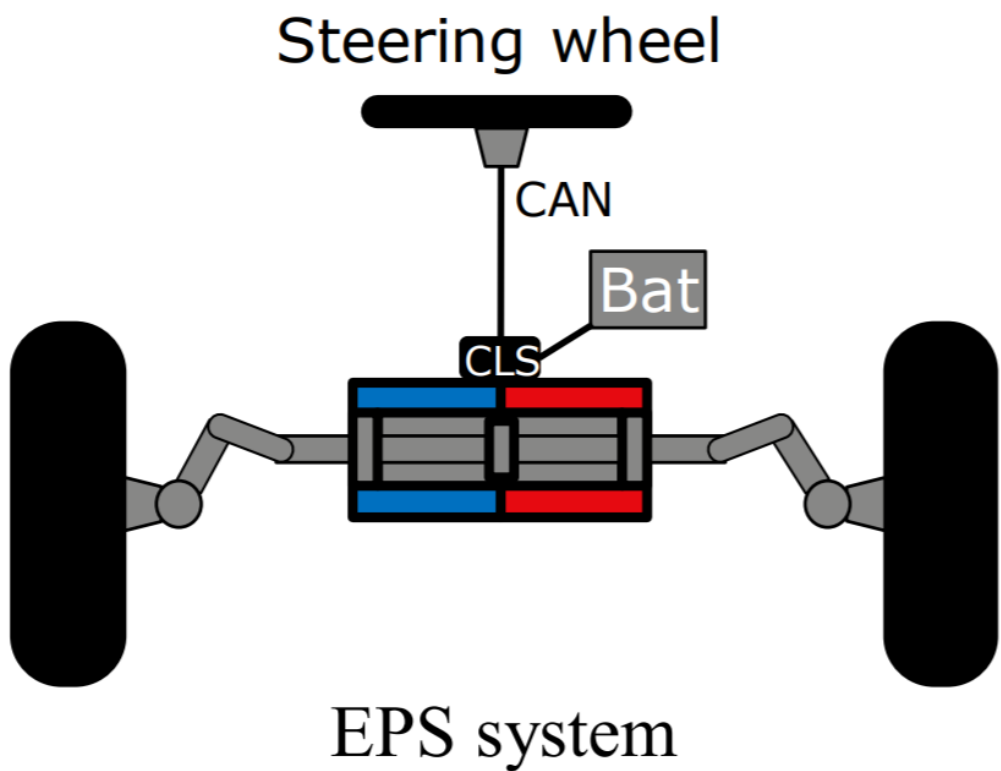


Mini Steering Wheel with Accurate Position Detection



P8 PROJECT
GROUP PED2-841
ENERGY TECHNOLOGY
AALBORG UNIVERSITY
MAY 28TH 2018

Title:

Mini Steering Wheel with Accurate Position Detection

Project:

P8-project

Project period:

February 2018 - May 2018

Project group:

PED2-841

Participants:

Christian Valentin
Mads Kousgaard Madsen
Mikkel Andri Hedemann

Supervisors:

Dong Wang
Kaiyuan Lu

Synopsis:

An increased development within electrification of transportation and focus on environmental health and safety has led to the investigation of sensorless position estimation, with the purpose of improving the traditional steering input known today. The purpose of this report is to investigate different methods of sensorless control in order to determine those suitable for low or no speed, referring to the speed of the steering input. The machine model was derived and two different methods were chosen in order to investigate any limitations and possibilities. Both methods tested had positive result and were able to detect the position when simulated and tested in the drives laboratory. Additionally, it was concluded that the possibility of active force feedback was applicable for both methods.

Pages: 42

Appendices: 5

Handed-in: 28-05-2018

By accepting the request from the fellow student who uploads the study group's project report in Digital Exam System, you confirm that all group members have participated in the project work, and thereby all members are collectively liable for the contents of the report. Furthermore, all group members confirm that the report dose not include plagiarism.

Preface

Reading Guide

Each chapter is introduced and finished by a short paragraph written in *italic* form. These paragraphs are introductions and partial conclusions for the given chapters. There will appear source references through the report. These references will be collected in a source list at the end of the report. The reference method used in the report is the Harvard Method which means that the reference is placed in the text with following notation [Surname, Year]. If the reference contains multiple sources, then each source is separated by comma. The references refer to the list of sources where books is stated with author, title, publisher, edition and year of publication while web pages is stated with author, web address, title and the point of time that indicates the last visit at the web page. Equations, tables and figures are numbered in accordance with the given chapter, i.e. Figure 1.2 is the second figure in chapter one. Explanatory text for figures and tables is located beneath the given tables and figures.

Christian Valentin

Mads Kousgaard Madsen

Mikkel Andri Hedemann

Nomenclature

DC	Direct Current	
DSP	Digital Signal Processor	
ECU	Electronic Control Unit	
EMF	Electromotive Force	
EPS	Electric Power Steering	
EV	Electric Vehicle	
FIR	Finite Impulse Response	
FOC	Field-oriented Control	
HF	High Frequency	
IIR	Infinite Impulse Response	
MCU	Micro Controller Unit	
PI	Proportional Integral	
PLL	Phase-locked Loop	
PM	Permanent Magnet	
PWM	Pulse Width Modulation	
SVPWM	Space Vector Pulse Width Modulation	
λ	Flux linkage	[Φ]
ω	Rotational speed	[rad/s]
τ	Time constant	[s]
θ	Angle	[$^{\circ}$]
ζ	Damping factor	[]
B	Bandwidth	[rad/s]
f	Frequency	[Hz]
I	Current	[A]
L	Inductance	[H]
R	Resistance	[Ω]

T	Torque	[Nm]
t	time	[s]
V	Voltage	[V]
w_n	Natural frequency	[rad/s]

Table of contents

Chapter 1 Introduction	1
1.1 Background	1
1.2 Sensorless Control Techniques	2
Chapter 2 Problem Statement	4
Chapter 3 Machine Modeling	5
Chapter 4 Position Detection	8
4.1 High Frequency Sinusoidal Voltage Injection	8
4.1.1 Alternative Position Detection Using HF Sinusoidal Voltage Injection	11
4.2 Voltage Pulse Injection	14
Chapter 5 Test and Validation	18
5.1 Lab Setup	18
5.2 Motor Parameter Determination	19
5.3 High Frequency Sinusoidal Voltage Injection	21
5.3.1 Results	22
5.4 Voltage Pulse Injection	24
5.4.1 Results	24
Chapter 6 Active Force Feedback	28
6.1 Current Controller Design	30
6.2 Implementation of Force Feedback for Sinusoidal Injection	33
6.3 Implementation of Force Feedback for Voltage Pulse Injection	34
Chapter 7 Conclusion	36
Chapter 8 Further work	39
8.1 Improvement of Measurement Accuracy	39
8.2 Digital Filter Design	39
8.3 Minimize Inverter Voltage Error	40
8.4 Reduction of Acoustic Noise	41
8.5 Implementation of Active Force Feedback	41
Bibliography	42
Appendix A Analog to Digital Conversion	43
Appendix B Digital Filter Implementation	46

Introduction

1

1.1 Background

In recent years electric vehicles (EVs) have seen a steady rise in popularity in public and personal transportation. The rise in popularity is due to the big advantages of EVs with respect to carbon dioxide emission as no fossil fuel is consumed. Furthermore, EVs can be charged by renewable resources.

Because of the growing interest in EVs, car manufacturers are looking to improve the reliability of their vehicles. One area of interest could be the electric power steering (EPS) system. Today the EPS system is implemented as seen in Figure 1.1.

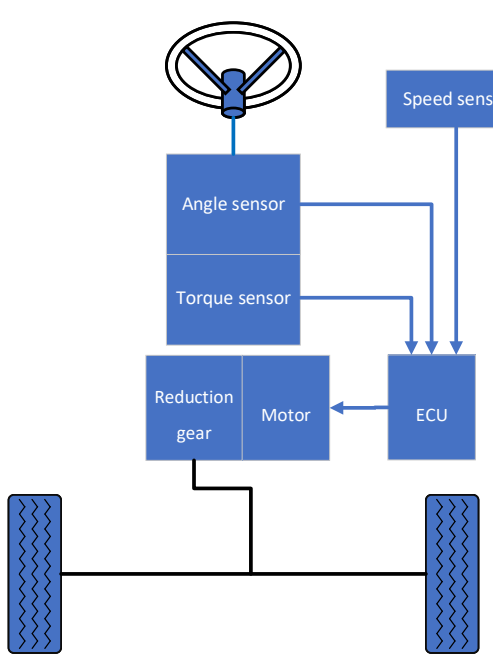


Figure 1.1. EPS system.

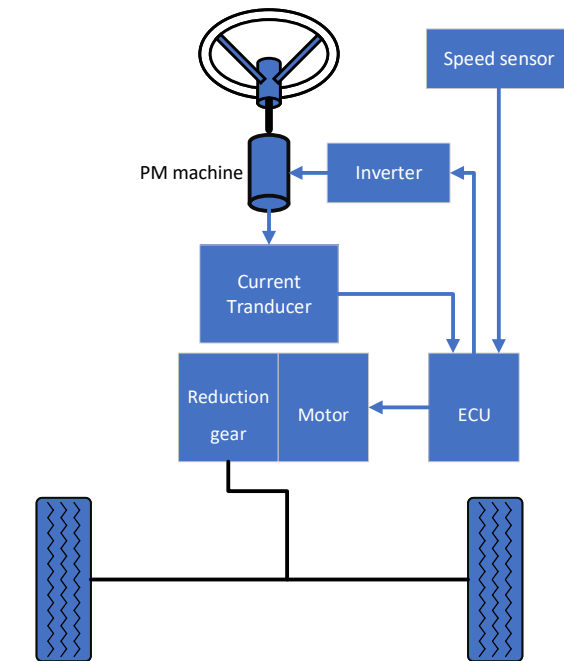


Figure 1.2. Improved EPS system.

From the figure it is seen that the electronic control unit (ECU) needs both torque and steering angle input from the steering wheel in order to determine the position reference that needs to be applied to the motor.

To improve this system and make it more reliable, the angle and torque sensor could be supplemented with sensorless control, to increase the reliability. Sensorless control uses current transducers to estimate the rotor position of a permanent magnet (PM) machine

connected to the steering column. The upside to this approach is the increased reliability of the system. A downside could however be the increased complexity, as certain algorithms need to be implemented in the ECU in order to accurately determine the rotor angle. Furthermore, as a PM machine is connected to the steering column, active force feedback can be applied, giving both control of the steering wheel position and feeling of the wheel position. The sensorless control diagram can be seen in Figure 1.2.

One of the main advantages associated with sensorless control with respect to steering, is the possibility to remove the steering column on off-highway vehicles. Removing the steering column would allow the designer to rethink the steering wheel and replace it with a joystick, or other alternative steering inputs. By doing so the designer could place the driver's seat close to the window of large combine machines, in order to both allow a better field of view, and a more ergonomic position as the driver would need to stretch less in order to get full overview.

Additionally, as the control and position detection is handled by a ECU, it is possible to do active force feedback, which enables the user or designer to fully configure the force felt by the user when turning the steering device. The use of ECU also allows the user/designer to change the sensitivity of the steering.

The sensorless position detection could also be used to replace the encoder on applications where weight is a concern. Drones are an example, where weight is an important factor with respect to flight time, as the needed current can be reduced thereby prolonging the flight time.

Throughout this section several applications have been presented, with respect to sensorless control. This report will examine the application for steering input detection. In the next section, a discussion of the sensorless control methods that exist will be presented with the purpose of determining suitable ones for the improved EPS system.

1.2 Sensorless Control Techniques

This section will give a brief overview of several existing sensorless control techniques. Since this application will be working at low or no speed at all, the control technique should work under these conditions.

Fundamental frequency position detection

For back-EMF control, the back-EMF of the motor is measured and used to determine the position error of the motor. This is done by setting the reference frame slightly off the actual position of the dq-axis, and estimating the position and speed from the measured voltage. However, for this technique a rotor speed is necessary in order to generate a voltage to measure. Hence, this is not suitable for low or no speed conditions.[Sungmin Kim]

High frequency position detection

At low or no speed, the saliency based voltage injection methods can be used. The idea is to determine the rotor position from the inductance due to the saliency of the magnetic path. This is done by injecting a high frequency voltage signal, which is then demodulated in order to determine the position. Several signal injection methods exists. Notably, there is the injection of a HF rotating vector, or injection of a voltage impulse. The main difference between the two, is that the rotating vector does not rely on a specific injection position, whereas an impulse injection would rely on a specific voltage injection position and would therefore need the estimated position as feedback. Another difference is the injection signal, where the rotating vector would be a sine wave, and the impulse injection would be a square wave.[Sungmin Kim]

From this section it can be concluded that a high frequency injection is be able to detect the position of the PM machine at low speeds. Distinct methods exists with fundamental differences of the injection voltage.

Problem Statement 2

In the introduction it was concluded that the electric power steering could be subject to improvement by implementing sensorless control. Several methods were reviewed and it was found that saliency based voltage injection could provide position feedback at low or no speed applications, where several signal injection methods exists. Additionally, a control scheme needs to be implemented for the machine connected to the steering. Therefore the project objectives are:

Project Objectives

- Derive the high frequency machine model of a permanent magnet machine.
- Investigate the sinusoidal injection method.
- Investigate the voltage pulse injection method.
- Validate the injection methods in the drive laboratory.
- Investigate active force feedback.
- Assess the performance of the sensorless control system.

Limitations and Assumptions

This project will only investigate the sensorless control methods, meaning that the modulation, control and non linearity of the inverter will not be examined.

Machine Modeling 3

In this chapter a high frequency low speed machine model will be derived in order to obtain a model, which can be used to determine the position of the rotor at low or no speed with high frequency voltage injections. The machine model will be derived in the estimated reference frame in order to investigate it further to determine the estimated rotor position.

For a permanent magnet machine, the voltage equation is given by [Paul Krause, 2013]

$$\bar{v}_{dq} = R\bar{i}_{dq} + \frac{d}{dt}\bar{\lambda}_{dq} + \omega_r \begin{bmatrix} 0 & -1 \\ 1 & 0 \end{bmatrix} \begin{bmatrix} \lambda_d \\ \lambda_q \end{bmatrix} \quad (3.1)$$

where \bar{v}_{dq} , \bar{i}_{dq} are the stator dq-axis voltage and current vectors, R is the stator resistance, ω_r is the rotor speed, and λ_{dq} is the dq-axis flux linkage, given by

$$\begin{bmatrix} \lambda_d \\ \lambda_q \end{bmatrix} = \begin{bmatrix} L_d & 0 \\ 0 & L_q \end{bmatrix} \begin{bmatrix} i_d \\ i_q \end{bmatrix} + \begin{bmatrix} \lambda_{mpm} \\ 0 \end{bmatrix} \quad (3.2)$$

where L_d and L_q are the d- and q-axis inductances, and λ_{mpm} is the peak value of the rotor flux linkage.

Due to the possibility of having a position error, it is needed to transform Equation (3.2) from the real dq-reference frame to an estimated dq-reference frame. The real and estimated reference frames are illustrated in Figure 3.1.

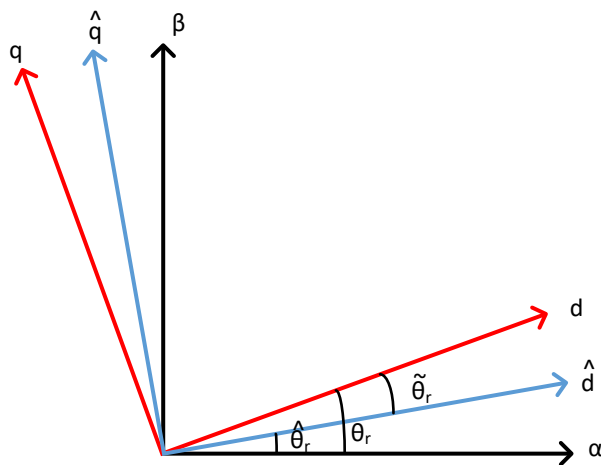


Figure 3.1. Real and estimated dq-reference frame.

In Figure 3.1 two dq-reference frames can be observed, where

- f corresponds to the real variable
- \hat{f} corresponds to the estimated variable
- \tilde{f} corresponds to the error variable

The real reference frame has the angle θ_r from phase-a or α in the stationary reference frame, and the estimated reference frame has the angle $\hat{\theta}_r$, which therefore introduces the angle of the position error as $\tilde{\theta}_r$. Using vector projection the real vector from the estimated vector and the position error can be determined as shown in Equation (3.3), or the other way around as shown in Equation (3.4).

$$\bar{f}_{dq} = \hat{f}_{dq} e^{-j\tilde{\theta}_r} \quad (3.3)$$

$$\hat{f}_{dq} = \bar{f}_{dq} e^{j\tilde{\theta}_r} \quad (3.4)$$

As known, Euler's formula states

$$e^{j\tilde{\theta}_r} = \cos \tilde{\theta}_r + j \sin \tilde{\theta}_r \quad \text{and} \quad e^{-j\tilde{\theta}_r} = \cos \tilde{\theta}_r - j \sin \tilde{\theta}_r \quad (3.5)$$

The vector projections can be written as

$$\begin{bmatrix} f_d \\ f_q \end{bmatrix} = \begin{bmatrix} \cos \tilde{\theta}_r & \sin \tilde{\theta}_r \\ -\sin \tilde{\theta}_r & \cos \tilde{\theta}_r \end{bmatrix} \begin{bmatrix} \hat{f}_d \\ \hat{f}_q \end{bmatrix} \triangleq K_{re} \begin{bmatrix} \hat{f}_d \\ \hat{f}_q \end{bmatrix} \quad (3.6)$$

$$\begin{bmatrix} \hat{f}_d \\ \hat{f}_q \end{bmatrix} = \begin{bmatrix} \cos \tilde{\theta}_r & -\sin \tilde{\theta}_r \\ \sin \tilde{\theta}_r & \cos \tilde{\theta}_r \end{bmatrix} \begin{bmatrix} f_d \\ f_q \end{bmatrix} \triangleq K_{er} \begin{bmatrix} f_d \\ f_q \end{bmatrix} \quad (3.7)$$

where the two transformation matrices are written as K_{re} and K_{er} for simplicity.

First, the flux linkage equation is transformed to the estimated reference frame as shown in Equation (3.8).

$$\hat{\lambda}_{dq} = K_{er} \bar{\lambda} = \begin{bmatrix} L_1 + L_2 \cos 2\tilde{\theta}_r & L_2 \sin 2\tilde{\theta}_r \\ L_2 \sin 2\tilde{\theta}_r & L_1 - L_2 \cos 2\tilde{\theta}_r \end{bmatrix} \begin{bmatrix} \hat{i}_d \\ \hat{i}_q \end{bmatrix} + \begin{bmatrix} \cos \tilde{\theta}_r \lambda_{mpm} \\ \sin \tilde{\theta}_r \lambda_{mpm} \end{bmatrix} \quad (3.8)$$

where $L_1 = (L_d + L_q)/2$ and $L_2 = (L_d - L_q)/2$.

By multiplying the voltage equation with the transformation matrix, K_{er} , the estimated machine model becomes

$$\hat{v}_{dq} = R \hat{i}_{dq} + K_{er} \frac{d}{dt} \bar{\lambda}_{dq} + \omega_r \begin{bmatrix} 0 & -1 \\ 1 & 0 \end{bmatrix} \begin{bmatrix} \hat{\lambda}_d \\ \hat{\lambda}_q \end{bmatrix} \quad (3.9)$$

The product rule for differential equations states that $\frac{d}{dt}(f(x)g(x)) = \frac{df(x)}{dt}g(x) + f(x)\frac{dg(x)}{dt}$, which means that the derivative term can be written as

$$K_{er} \frac{d}{dt} \bar{\lambda}_{dq} = \frac{d}{dt}(K_{er} \bar{\lambda}_{dq}) - \frac{d}{dt}(K_{er}) \bar{\lambda}_{dq} \quad (3.10)$$

As $K_{er}\bar{\lambda}_{dq} = \hat{\lambda}_{dq}$ and $K_{er}K_{re} = 1$, the derivative term can be written as

$$K_{er} \frac{d}{dt} \bar{\lambda}_{dq} = \frac{d}{dt} \hat{\lambda}_{dq} - \frac{d}{dt} (K_{er}) K_{re} K_{er} \bar{\lambda}_{dq} \quad (3.11)$$

The term $\frac{d}{dt} (K_{er}) K_{re}$ can be simplified as

$$\begin{aligned} \frac{d}{dt} (K_{er}) K_{re} &= \frac{d}{dt} \left(\begin{bmatrix} \cos \tilde{\theta}_r & -\sin \tilde{\theta}_r \\ \sin \tilde{\theta}_r & \cos \tilde{\theta}_r \end{bmatrix} \right) \begin{bmatrix} \cos \tilde{\theta}_r & \sin \tilde{\theta}_r \\ -\sin \tilde{\theta}_r & \cos \tilde{\theta}_r \end{bmatrix} \\ &= \tilde{\omega}_r \begin{bmatrix} -\sin \tilde{\theta}_r & -\cos \tilde{\theta}_r \\ \cos \tilde{\theta}_r & -\sin \tilde{\theta}_r \end{bmatrix} \begin{bmatrix} \cos \tilde{\theta}_r & \sin \tilde{\theta}_r \\ -\sin \tilde{\theta}_r & \cos \tilde{\theta}_r \end{bmatrix} = \tilde{\omega}_r \begin{bmatrix} 0 & -1 \\ 1 & 0 \end{bmatrix} \end{aligned} \quad (3.12)$$

Therefore, the final equation for the estimated voltage becomes

$$\hat{v}_{dq} = R\hat{i}_{dq} + \frac{d}{dt} \hat{\lambda}_{dq} + \hat{\omega}_r \begin{bmatrix} 0 & -1 \\ 1 & 0 \end{bmatrix} \begin{bmatrix} \hat{\lambda}_d \\ \hat{\lambda}_q \end{bmatrix} = R\hat{i}_{dq} + \frac{d}{dt} \hat{\lambda}_{dq} + j\hat{\omega}_r \hat{\lambda}_{dq} \quad (3.13)$$

In order to derive the low speed machine model, the flux linkage equation is presented in a vector form as real and imaginary part, $\bar{f}_{dq} = f_d + jf_q$. It therefore becomes as follows

$$\begin{aligned} \hat{\lambda}_{dq} &= L_1(\hat{i}_d + j\hat{i}_q) + L_2\left(\hat{i}_d \cos 2\tilde{\theta}_r + \hat{i}_q \sin 2\tilde{\theta}_r + j\hat{i}_d \sin 2\tilde{\theta}_r - \hat{i}_q \cos 2\tilde{\theta}_r\right) + \lambda_{mpm} e^{j\tilde{\theta}_r} \\ &= L_1 \hat{i}_{dq} + L_2(\hat{i}_d - j\hat{i}_q)(\cos 2\tilde{\theta}_r + j \sin 2\tilde{\theta}_r) + \lambda_{mpm} e^{j\tilde{\theta}_r} \\ &= L_1 \hat{i}_{dq} + L_2 \hat{i}_{dq}^* e^{j2\tilde{\theta}_r} + \lambda_{mpm} e^{j\tilde{\theta}_r} \end{aligned} \quad (3.14)$$

where \hat{i}_{dq}^* is the complex conjugate of the dq-axis current. The derivative of the flux linkage becomes in vector as follows

$$\begin{aligned} \frac{d}{dt} \hat{\lambda}_{dq} &= \frac{d}{dt} (L_1 \hat{i}_{dq} + L_2 \hat{i}_{dq}^* e^{j2\tilde{\theta}_r} + \lambda_{mpm} e^{j\tilde{\theta}_r}) \\ &= L_1 \frac{d\hat{i}_{dq}}{dt} + L_2 \frac{d\hat{i}_{dq}^*}{dt} e^{j2\tilde{\theta}_r} + j2\tilde{\omega}_r L_2 \hat{i}_{dq}^* e^{j2\tilde{\theta}_r} + j\tilde{\omega}_r \lambda_{mpm} e^{j\tilde{\theta}_r} \end{aligned} \quad (3.15)$$

Therefore the voltage equation becomes

$$\hat{v}_{dq} = R\hat{i}_{dq} + L_1 \frac{d\hat{i}_{dq}}{dt} + L_2 \frac{d\hat{i}_{dq}^*}{dt} e^{j2\tilde{\theta}_r} + j2\tilde{\omega}_r L_2 \hat{i}_{dq}^* e^{j2\tilde{\theta}_r} + j\tilde{\omega}_r \lambda_{mpm} e^{j\tilde{\theta}_r} + j\hat{\omega}_r \hat{\lambda}_{dq} \quad (3.16)$$

In $\alpha\beta$ -reference frame, where $\hat{\omega}_r = 0$ and $\hat{\theta}_r = 0$, the voltage equation becomes

$$\hat{v}_{\alpha\beta} = R\hat{i}_{\alpha\beta} + L_1 \frac{d\hat{i}_{\alpha\beta}}{dt} + L_2 \frac{d\hat{i}_{\alpha\beta}^*}{dt} e^{j2\theta_r} + j2\omega_r L_2 \hat{i}_{\alpha\beta}^* e^{j2\theta_r} + j\omega_r \lambda_{mpm} e^{j\theta_r} \quad (3.17)$$

From the voltage equation, it can be observed that information regarding the position can be obtained either from $j\omega_r \lambda_{mpm} e^{j\theta_r}$, which is the back-EMF, or from the two L_2 -terms. As mentioned previously, the rotor will be moving at low speed, which means that the rotational speed, ω_r , ideally will be zero. This means that the two last terms of the voltage equation are negligible. Furthermore, the impedance of the inductances will be high due to the high frequency voltage injection, making the resistance-term small and negligible.

The resulting HF low speed machine model therefore becomes

$$\hat{v}_{\alpha\beta} = L_1 \frac{d\hat{i}_{\alpha\beta}}{dt} + L_2 \frac{d\hat{i}_{\alpha\beta}^*}{dt} e^{j2\theta_r} \quad (3.18)$$

Position Detection 4

In this chapter, various high frequency injection methods will be presented and analyzed in order to estimate the rotor position at low speed or no speed. First, a sinusoidal injection method will be analyzed, where two methods used to extracting the position will be presented. Then, a square wave voltage pulse injection will be analyzed. These models will be implemented and tested in the MATLAB simulation software, Simulink, in order to determine suitable methods for the project application. The simulations done in this chapter has been made using generic motor parameters in order to test the performance of the methods.

4.1 High Frequency Sinusoidal Voltage Injection

In this section the high frequency sinusoidal voltage injection method will be explained. The purpose of this method is to inject a rotating voltage vector at a high frequency into the PM machine, which will then give an output current, including several different frequency components. By filtering the high frequency current components, the electrical rotor position can be directly extracted. The mathematical expressions will be presented in order to explain how the position can be estimated.

As derived in Chapter 3, the low speed machine model is

$$\bar{v}_{\alpha\beta h} = L_1 \frac{d\bar{i}_{\alpha\beta h}}{dt} + L_2 \frac{d\bar{i}_{\alpha\beta h}^*}{dt} \cdot e^{j2\theta_r} \quad (4.1)$$

where the subscript h is a notation for the high frequency signal. The low speed model can be expanded as follows

$$\begin{bmatrix} v_{\alpha h} \\ v_{\beta h} \end{bmatrix} = \begin{bmatrix} L_1 + L_2 \cos 2\theta_r & L_2 \sin 2\theta_r \\ L_2 \sin 2\theta_r & L_1 - L_2 \cos 2\theta_r \end{bmatrix} \frac{d}{dt} \begin{bmatrix} i_{\alpha h} \\ i_{\beta h} \end{bmatrix} \quad (4.2)$$

The voltage is chosen to be injected as a rotating vector, which rotates clockwise at a high frequency, where V_h is the amplitude of the high frequency voltage injection and ω_h is the frequency.

$$\begin{bmatrix} v_{\alpha h} \\ v_{\beta h} \end{bmatrix} = V_h \begin{bmatrix} \sin \omega_h t \\ \cos \omega_h t \end{bmatrix} \quad (4.3)$$

By injecting this voltage vector and solving for i_α and i_β , a general solution can be found

$$\begin{cases} i_{\alpha h} = \frac{V_h}{(L_1^2 - L_2^2)\omega_h} (L_2 \cos(\theta_h + 2\theta_r) - L_1 \cos \theta_h) \\ i_{\beta h} = \frac{V_h}{(L_1^2 - L_2^2)\omega_h} (L_2 \sin(\theta_h + 2\theta_r) + L_1 \sin \theta_h) \end{cases} \quad (4.4)$$

If a fundamental component is additionally given to the PM machine in order to make it rotate, the total current becomes

$$\begin{cases} i_\alpha = k_1(L_2 \cos(\theta_h + 2\theta_r) - L_1 \cos \theta_h) + k_2 \cos(\omega_e t + \phi) \\ i_\beta = k_1(L_2 \sin(\theta_h + 2\theta_r) + L_1 \sin \theta_h) + k_2 \sin(\omega_e t + \phi) \end{cases} \quad (4.5)$$

where $k_1 = \frac{V_h}{(L_1^2 - L_2^2)\omega_h}$ and $k_2 \sin(\omega_e t + \phi)$ is the fundamental current rotating at the electrical frequency of $2\pi\omega_e$ and has amplitude of k_2 . In vector form it becomes

$$\bar{i}_{\alpha\beta} = k_1(L_2 e^{j(\theta_h + 2\theta_r)} - L_1 e^{-j\theta_h}) + k_2 e^{j(\omega_e t + \phi)} \quad (4.6)$$

Now, by transforming this $\alpha\beta$ current to the high frequency dq-reference frame using the angle of the high frequency injection, the following current can be obtained

$$\bar{i}_{dq} = k_1(L_2 e^{j(2\theta_r)} - L_1 e^{-j(2\theta_h)}) + k_2 e^{j(\omega_e t + \phi - \theta_h)} \quad (4.7)$$

As it can be seen in Equation (4.7), the dq-reference current, which is obtained, contains three components. One term will be rotating at a speed of $2\omega_r$ and the other two terms will be rotating at $2\omega_h$ and $\omega_e - \omega_h$ respectively. As θ_r has a frequency which is significantly lower than θ_h , the high frequency signals can be filtered using a low-pass filter, leaving only the component containing θ_r . This component can then be demodulated in order to obtain the real rotor position θ_r . In Figure 4.1 a block diagram is shown, where a possible way of implementing the position detection method is presented.

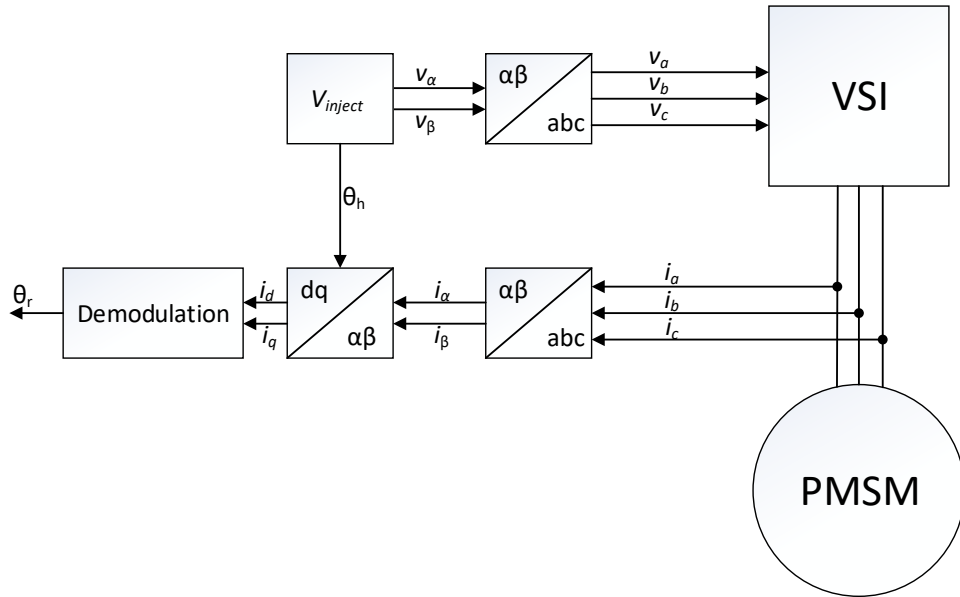


Figure 4.1. Block diagram of a possible way to implement the high frequency sinusoidal voltage injection method.

This method is implemented in Simulink in order to validate the method. In Figure 4.2 the result of the position detection is shown. In the simulation the injection voltage has a magnitude of 10 V and a frequency of 500 Hz.

It can be observed that at 0.5 seconds the reference angle is given a ramp from zero to 90 degrees, where the estimated position is seen to follow the ramp with a small error. This might be due to the fact that in the Simulink model, the resistance is included. The position detection method is therefore tested with the machine resistance varying from 0.2Ω to 1Ω . In Figure 4.3 the electrical position error can be observed in the interval around and during the speed ramp. It can be observed that the error is proportional to the resistance. When the resistance is 0.6Ω the electrical position error is around 1° . However, the voltage drop over the resistance can be minimized compared to the voltage drop across the inductances by increasing the frequency of the injection signal as it will result in a higher impedance of the inductances.

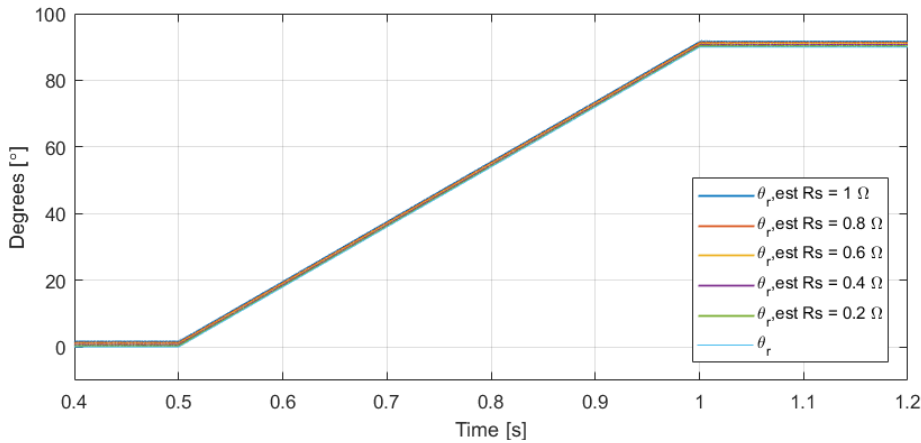


Figure 4.2. Simulink simulation of position detection using high frequency sinusoidal voltage injection method with varying machine resistance.

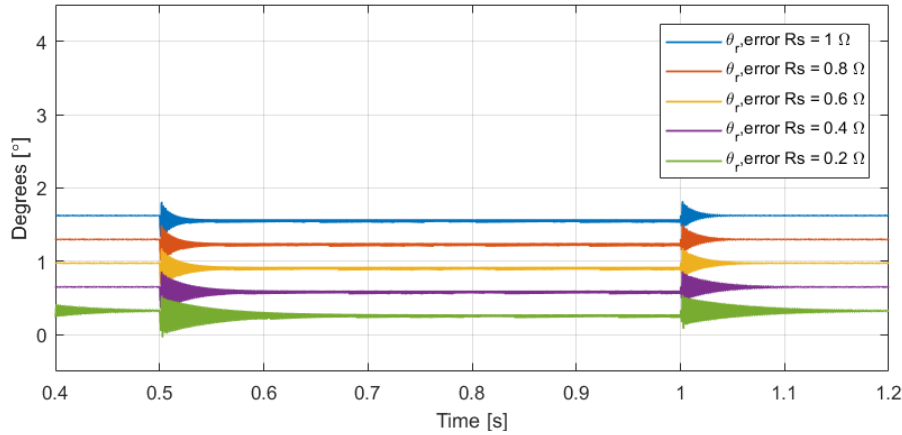


Figure 4.3. Simulink simulation of electrical position error using high frequency sinusoidal voltage injection method with varying machine resistance.

In Figure 4.4 and 4.5 the simulation results of the position detection method are presented, where the voltage injection has an amplitude of 10 V and varying frequency. The machine resistance is set as 0.78Ω for this simulation. As previously stated, it can be observed that the error is reduced when increasing the frequency of the voltage injection.

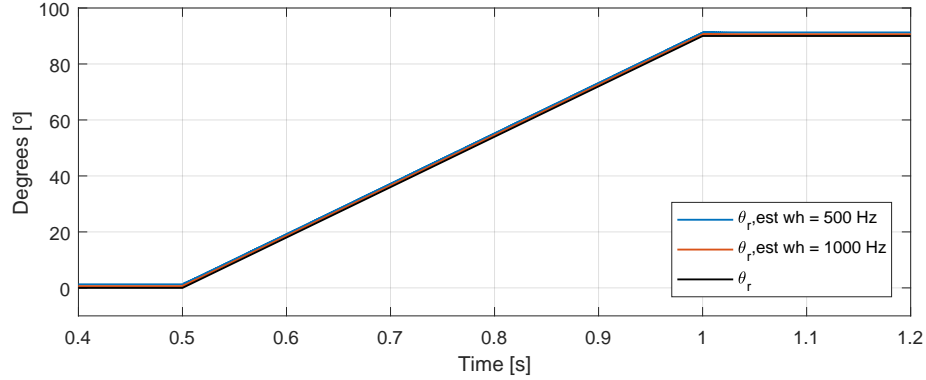


Figure 4.4. Simulink simulation of position detection using high frequency sinusoidal voltage injection method with varying injection frequency.

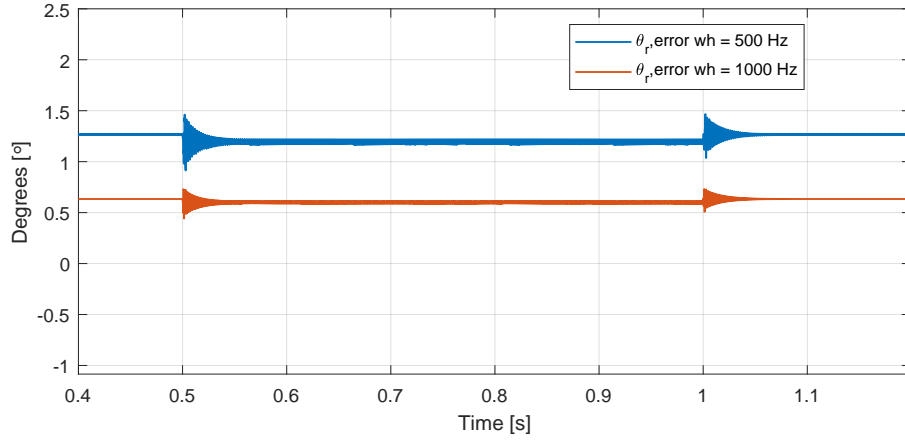


Figure 4.5. Simulink simulation of electrical position error using high frequency sinusoidal voltage injection method with varying injection frequency.

It should be noted that the amplitude of the component, which includes $2\theta_r$, is inverse proportional to ω_h as $k_1 = \frac{V_h}{(L_1^2 - L_2^2)\omega_h}$. This means that when the frequency is increased, the amplitude will decrease and therefore might become difficult to measure. This can be counter measured by increasing the amplitude of the injection voltage.

A disadvantage of this high frequency method is the need of a filter. The filter can result in delay of the signals and a decreased bandwidth, which are unwanted. An alternative method of extracting the position will therefore be presented.

4.1.1 Alternative Position Detection Using HF Sinusoidal Voltage Injection

Looking at the $\alpha\beta$ -currents in Equation (4.5) it is possible to extract the position without using a filter through some mathematical equation manipulation. As no fundamental current is injected, the fundamental current component, $k_2 \sin(\omega_e t + \phi)$, is neglected. The

currents then become

$$\begin{cases} i_\alpha = k_1(L_2 \cos(\theta_h + 2\theta_r) - L_1 \cos\theta_h) \\ i_\beta = k_1(L_2 \sin(\theta_h + 2\theta_r) + L_1 \sin\theta_h) \end{cases} \quad (4.8)$$

By multiplying i_α with $\sin\theta_h$ and i_β with $\cos\theta_h$ and adding the two current together, Equation (4.9) is obtained.

$$i_\alpha \sin\theta_h + i_\beta \cos\theta_h = k_1 L_2 \cos(\theta_h + 2\theta_r) \sin\theta_h + k_1 L_2 \sin(\theta_h + 2\theta_r) \cos\theta_h \quad (4.9)$$

The following trigonometric relation is known

$$\sin(A + B) = \sin(A)\cos(B) + \cos(A)\sin(B) \quad (4.10)$$

Equation (4.9) can therefore be reduced to

$$i_\alpha \sin\theta_h + i_\beta \cos\theta_h = k_1 L_2 \sin(2\theta_h + 2\theta_r) \quad (4.11)$$

It can then be observed that when Equation (4.11) equals zero, it is known that $\theta_r + \theta_h$ should be equal to either zero or π . Therefore

$$\theta_r + \theta_h = 0 \Rightarrow \theta_r = -\theta_h \quad (4.12)$$

Hence the position can be directly estimated by sampling the high frequency position.

In Simulink this method is implemented in a similar way as the previous method meaning that the injection voltage has an amplitude of 10 V and a frequency of 500 Hz. The only difference is how the measured $\alpha\beta$ -currents are analyzed. In this method the equations are manipulated as mentioned and every second time Equation (4.11) equals zero a trigger is given to θ_h , which then directly gives the electrical rotor position with the opposite polarity.

In Figure 4.1 the result of this position detection method is shown. Similarly to the previous method a ramp is given at 0.5 second, where the reference angle goes from zero to 90° . It can be seen that an error is present as previously. Due to the limits of the position being between zero and 2π , the measured position is just below 360° instead of zero. In Figure 4.7 the electrical position error is presented. It can be observed that the electrical position error is significantly larger compared to the previous method. With the machine resistance at 0.6Ω , the error is 3° whereas it was 1° with the previous method.

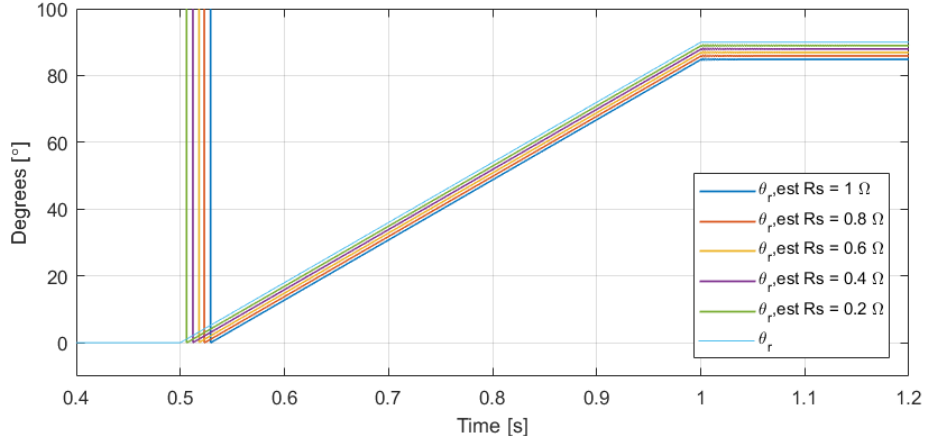


Figure 4.6. Simulink simulation of position detection using high frequency AC voltage injection method without a filter.

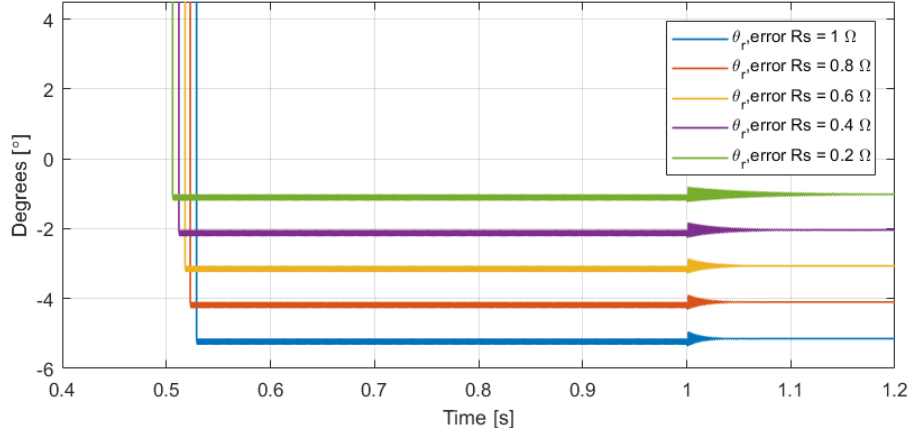


Figure 4.7. Simulink simulation of electrical position error using high frequency AC voltage injection method.

Although this detection can be implemented in a simulation without a filter, issues may occur in digital implementation. One possible issue is the fact that the DSP measures digitally, meaning that it does not measure continuously. Hence there is a risk of not measuring exactly when Equation (4.11) equals zero and therefore not estimating the exact value of the position creating an error. Another possible issue is that in real implementation, noise from other sources, for example the inverter, can occur and will result in measurement errors. In order to prevent noise, a low-pass filter can be implemented.

As this position detection method also has a need of a filter and has a higher position error, it is not preferred compared to the previous high frequency method. Furthermore, due to the fundamental component being neglected, the method can not be used for FOC.

4.2 Voltage Pulse Injection

The voltage pulse injection method is used to estimate the rotor position of a PM machine at low speed and standstill by injecting a single controllable voltage pulse, causing a variation in the machine output current. This current variation is directly linked to the position error and is reliable which means that, unlike the high frequency rotating vector method, there is no need for a filter. In this section the theory behind this voltage pulse method is presented. Furthermore, the method is implemented in Simulink in order to verify that it works in theory.

As previously stated the low speed machine model can be presented as

$$\bar{v}_{\alpha\beta} = L_1 \frac{d\bar{i}_{\alpha\beta}}{dt} + L_2 \frac{d\bar{i}_{\alpha\beta}^*}{dt} \cdot e^{j2\theta_r} \quad (4.13)$$

By solving for $\frac{d\bar{i}_{\alpha\beta}}{dt}$, the machine model becomes

$$\frac{d\bar{i}_{\alpha\beta}}{dt} = \frac{1}{L_1^2 + L_2^2} (L_1 \bar{v}_{\alpha\beta} - L_2 \bar{v}_{\alpha\beta}^* \cdot e^{j2\theta_r}) \quad (4.14)$$

One of the assumptions of the voltage pulse method is that for one switching period, the current variation, $\frac{d\bar{i}_{\alpha\beta}}{dt}$, can be solved as $\frac{\Delta\bar{i}_{\alpha\beta}}{\Delta t}$, which is determined as

$$\begin{aligned} \Delta\bar{i}_{\alpha\beta} &= \left(\frac{L_1}{L_1^2 - L_2^2} + \frac{-L_2}{L_1^2 - L_2^2} \cdot e^{j2(\theta_r - \theta_v)} \right) \cdot \Delta t \cdot \bar{v}_{\alpha\beta} \\ &= \left(y + \Delta y \cdot e^{j2(\theta_r - \theta_v)} \right) \cdot \Delta t \cdot V_m e^{j\theta_v} \end{aligned} \quad (4.15)$$

The equation is then transformed from the $\alpha\beta$ -reference frame to the estimated dq-reference frame by using the the estimated position, $\hat{\theta}_r$, as shown in Equation (4.16), where $(\gamma\delta)$ is the estimated dq-reference frame. Figure 4.8 illustrates the three different reference frames and corresponding angles.

$$\Delta\bar{i}_{\gamma\delta} = \Delta\bar{i}_{\alpha\beta} e^{-j\hat{\theta}_r} = \left(y + \Delta y \cdot e^{j2(\theta_r - \hat{\theta}_r - (\theta_v - \hat{\theta}_r))} \right) \cdot \Delta t V_m \cdot e^{j\theta_v} e^{-j\hat{\theta}_r} \quad (4.16)$$

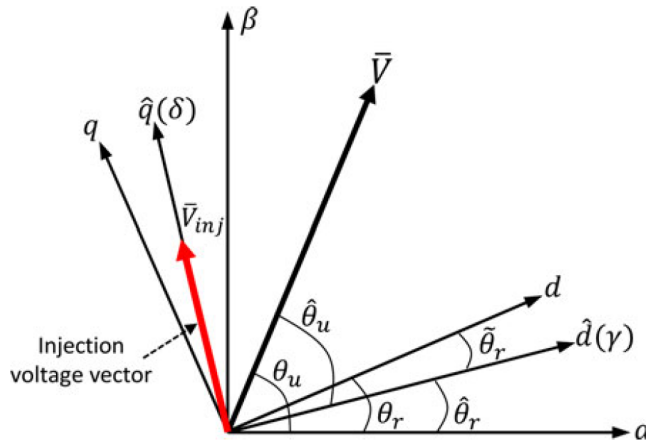


Figure 4.8. $\alpha\beta$ -reference frame, dq-reference frame, $\hat{d}\hat{q}(\gamma\delta)$ -reference frame (estimated) and corresponding angles θ_r (actual), $\hat{\theta}_r$ (estimated) and $\tilde{\theta}_r$ (error) [Ge Xie, 2016].

As $\theta_r - \hat{\theta}_r = \tilde{\theta}_r$ and $\theta_v - \hat{\theta}_r = \hat{\theta}_v$ the current difference becomes

$$\Delta \bar{i}_{\gamma\delta} = \left(y + \Delta y \cdot e^{j2(\tilde{\theta}_r - \hat{\theta}_v)} \right) \cdot \Delta t V_m \cdot e^{j\hat{\theta}_v} \quad (4.17)$$

By injecting a single voltage vector, which is aligned with the estimated q-axis, $\hat{\theta}_v = 90^\circ$, the error of the position can be determined as shown

$$\Delta \bar{i}_{\gamma\delta} = \left(y + \Delta y \cdot e^{j2(\tilde{\theta}_r - 90^\circ)} \right) \cdot \Delta t V_m \cdot e^{j90^\circ} \quad (4.18)$$

Using Euler's Formula, Equation (4.18) can be written as

$$\Delta \bar{i}_{\gamma\delta} = jy\Delta t V_m + j\Delta y\Delta t V_m (\cos(2\tilde{\theta}_r - 180^\circ) + j\sin(2\tilde{\theta}_r - 180^\circ)) \quad (4.19)$$

It can be observed from the equation that

$$Re(\Delta \bar{i}_{\gamma\delta}) = \Delta \bar{i}_\gamma = -\Delta y\Delta t V_m \sin(2\tilde{\theta}_r - 180^\circ) = \Delta y\Delta t V_m \sin(2\tilde{\theta}_r) \quad (4.20)$$

The position error, which can be obtained, is then fed to a PLL, which will be able to estimate the rotor position, $\hat{\theta}_r$, and the estimated rotor speed, $\hat{\omega}_r$.

As mentioned previously, the implementation of this method requires a voltage pulse injection. In Simulink a voltage is injected with an amplitude of 20 V. The sample frequency is 10 kHz, which means that the voltage will be on for 100 μs and off for 100 μs . This voltage is injected in the estimated q-axis. A trigger is then used to obtain the measured current just before and after the voltage pulse to get the current difference. Using the estimated position, the $\alpha\beta$ -reference frame current is transformed to the estimated dq-reference frame to obtain the real position error, which, as mentioned, is fed to a PLL. In order to obtain the rotor position fast and precisely, a well-designed PLL is needed.

Typically, a PLL is represented by a second order system and the transfer function is described as

$$G_{PLL}(s) = \frac{K_p s + K_i}{s^2 + K_p s + K_i} \quad (4.21)$$

The transfer function of a second order system is

$$G_{2nd}(s) = \frac{\omega_n^2}{s^2 + 2\zeta\omega_n s + \omega_n^2} \quad (4.22)$$

That means that K_p and K_i can be estimated as

$$K_p = 2\zeta\omega_n \quad \text{and} \quad K_i = \omega_n^2 \quad (4.23)$$

By specifying the damping ratio, ζ , and determining the bandwidth, the natural frequency, ω_n , can be determined. An optimally damped system has a damping ratio of about 0.7. As the bandwidth is inverse proportional to the risetime, a high bandwidth is wanted in order to increase the speed of the PLL. However, the bandwidth is limited by the sampling frequency, as it can amplify the switching noise if frequencies are too close to each other. As a rule of thumb, the bandwidth should be 0.1 times the switching or sampling frequency.

That means that the bandwidth is set to 1 kHz. By using Equation (4.24), the natural frequency, ω_n , can be approximated. [J.-L. Chen, 2009]

$$B_w = \frac{1}{t_r} \cong \frac{\omega_n}{(1.1 - 0.334\zeta)} \quad (4.24)$$

This results in the following PLL parameters

$$K_p = 4.27 \cdot 10^3 \quad \text{and} \quad K_i = 9.12 \cdot 10^6 \quad (4.25)$$

In Simulink this method is implemented with the PLL feeding the estimated position to the injection voltage and the dq-transformation, meaning that it is full sensorless. In Figure 4.9 the Simulink simulation result is shown. As it can be observed, a ramp is given at 0.5 second, which stops at 90° after 0.5 seconds. As the ramp starts, the effect of the rotation result in the position estimation dropping just below 0° , which is just under 360° due to the use of modulus. During the ramp, there is a constant position error as seen in Figure 4.10.

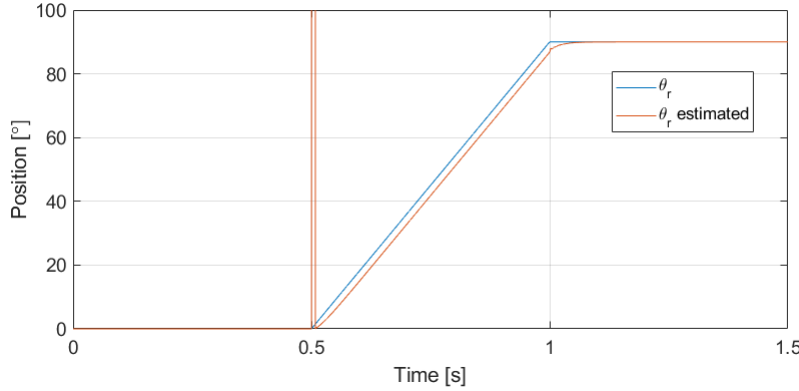


Figure 4.9. Simulink simulation of position estimation using voltage pulse injection method.

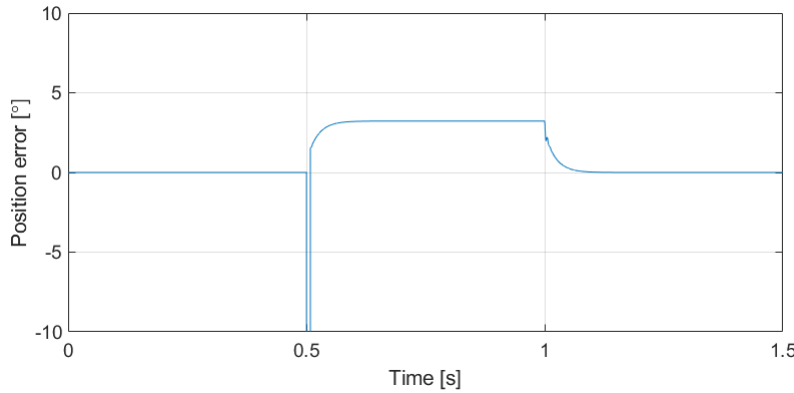


Figure 4.10. Simulink simulation of position estimation error using voltage pulse injection method.

In Figure 4.11 the simulation result is zoomed in at the end of the ramp, where the error during the ramp is shown. It can be observed, that the PLL gives a precise position estimation quickly after the ramp with no steady-state error.

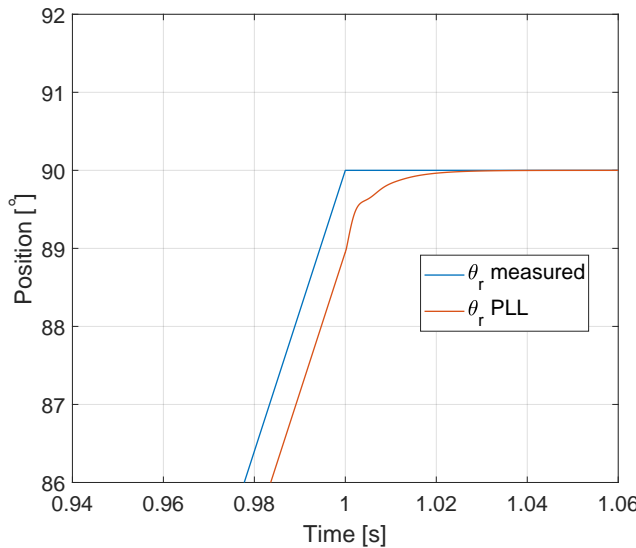


Figure 4.11. Simulink simulation of position estimation using the voltage pulse injection method zoomed in at the end of the ramp.

In conclusion both the high frequency sinusoidal voltage injection and the voltage pulse injection methods are viable solutions for this project. The sinusoidal voltage method has the benefit of being simple to implement and does not require a position feedback. However, it was seen that the position error is dependent on both the machine resistance and the injection frequency. Furthermore, a filter is needed, which results in a delay of the signal and decreases the bandwidth.

Another position extraction method was tested with the sinusoidal injection to analyze if the position could be extracted without a filter using a signal trigger. This trigger method had a higher position error and might have problems with a DSP setup. It is therefore not chosen to work with further.

Finally, the voltage pulse injection method has the benefit of not needing a filter as the voltage is injected in pulses. With the use of a well-designed PLL, a precise rotor position is estimated fast with no steady-state error, which makes it preferable for applications where a very precise position detection is needed. Both the sinusoidal voltage injection method and the voltage pulse injection method will be tested in the laboratory in the following chapter in order to further analyze pros and cons of each method.

Test and Validation

5

In this chapter the test and validation of the voltage injection methods will be performed and discussed. The chapter will present a description of the test bench and its subsystems. Furthermore, a motor parameter determination will be performed in order to get the correct parameters, representing the PM machine used for the test bench.

5.1 Lab Setup

In this section, the test bench for the test and validation will be presented. Each individual subsystem will be explained with respect to both functionality and purpose when testing and validating the methods described in Chapter 4.

As illustrated in Figure 5.1, the test bench consist of several subsystems with different purposes. In order to fully understand the extent of sensorless control with respect to actual implementation, it is necessary to identify and shortly describe each subsystem. This also helps identifying any possible malfunction and reduces debugging time.

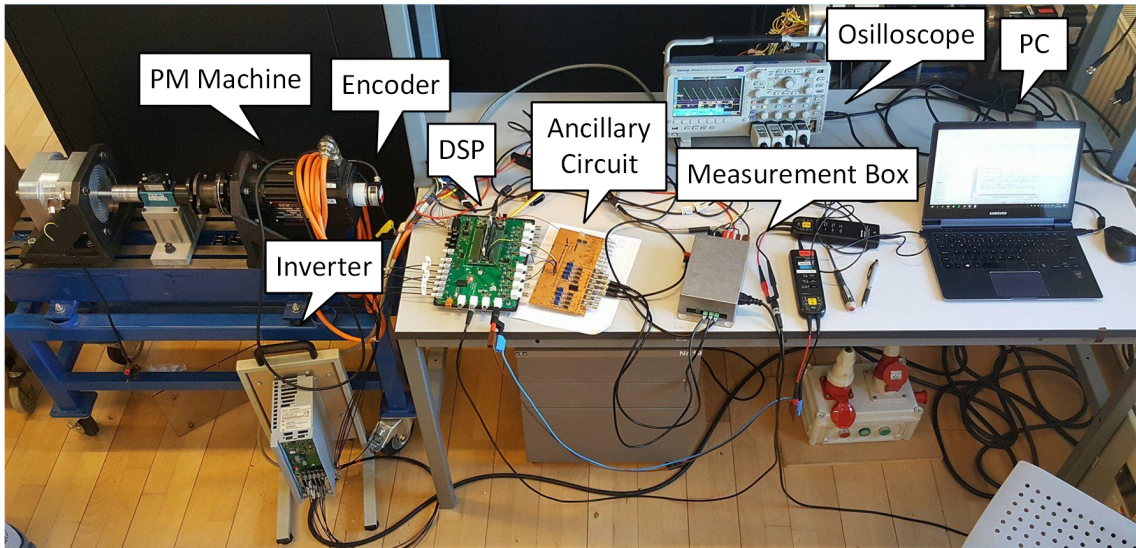


Figure 5.1. Test bench for sensorless position detection and active force feedback.

PC

The PC is considered as the control panel of the test bench and is used deploy the c-code onto the DSP and to monitor c-code output values.

DSP

The DSP is used to process input and output signals using the c-code provided by the PC.

Examples of input signals could be the encoder and analog to digital conversion (ADC) signals, whereas output signals could be those going to the inverter and digital to analog conversion (DAC).

Oscilloscope

The oscilloscope is used to display the signals from the DAC and probes. Displaying the signals onto the oscilloscope is an advantage since possible errors are easier detected.

Ancillary circuit

The ancillary circuit contains the ADC input and DAC output ports and the fiber optic connectors and is connected to the DSP. It can either be powered through a USB used to power the DSP, or by an external DC power supply.

Inverter

The inverter is used to generate any desired voltage input to the PM machine. The inverter is connected to the ancillary circuit and controlled by the DSP, which sends control signals through the fiber optic connectors. The control signals are generated using SVPWM.

Measurement Box

The measurement box is used to measure three phase currents. The output signals are current signals that are down scaled in order to comply with the voltage range of the ADC and DSP.

PM machine

The PM machine has 6 poles which dictates the conversion ratio, going from electrical to mechanical degrees and vice versa, and represents the PM machine placed on the steering column illustrated in Figure 1.2. It is used to test the methods of sensorless control by injecting special voltages and using current transducers to estimate the rotor position. The parameters of the PM machine, such as the resistance, inductance and flux linkage are used in simulink in order to be able to test and validate the methods of sensorless control described in Chapter 4.

Encoder

The encoder is attached on the shaft of the PM machine and is used to determine the error between the estimated and the real rotor position. The output of the encoder is connected to the AD input of the ancillary circuit sending it to the DSP where it is processed and finally displayed on the oscilloscope through the DA output.

5.2 Motor Parameter Determination

In order to validate the methods and increase the precision of the measurements, it is needed to determine the motor parameters of the PM machine used for the test bench. This includes the stator resistance and the dq-axis inductance, as the accuracy of the position detection methods depends upon these parameters, as stated in Chapter 4.

In practice the machine parameters can be determined by injecting a voltage in phase-a, which will be stepped. By short circuiting phase-b and -c measuring the current between phase-a and -b or -c in both the transient period and in the steady state it is possible to calculate the resistance and the inductance using Equations (5.1), (5.2) and (5.3), respectively.

When reaching steady state the resistance is easily obtained as $\frac{di}{dt} = 0$ and the magnitude

of V_{ab} equals the step input.

$$V_{ab} = \left(\frac{3}{2}\right) \cdot V_d = \left(\frac{3}{2} \cdot R\right)i_d + \left(\frac{3}{2} \cdot L_d\right)\frac{di_d}{dt} = \left(\frac{3}{2} \cdot R\right)i + \left(\frac{3}{2} \cdot L_d\right)\frac{di}{dt} \quad (5.1)$$

$$-V_{ab} = \left(\frac{3}{2}\right) \cdot V_q = \left(\frac{3}{2} \cdot R\right)i_q + \left(\frac{3}{2} \cdot L_q\right)\frac{di_q}{dt} = \left(\frac{3}{2} \cdot R\right)i + \left(\frac{3}{2} \cdot L_q\right)\frac{di}{dt} \quad (5.2)$$

The inductance however, can be obtained using Equation (5.3) that utilizes the time constant for a first order time response of a LR system to obtain the inductance. The time constant corresponds to the time it takes the current to reach 63 % of its steady state value.

$$\tau = \frac{L}{R} \quad (5.3)$$

However, due to rotor saliency, which the high frequency methods are based upon, it is needed to align the north pole of the rotor with phase-a in order to determine the d-axis inductance as illustrated in Figure 5.2, since $L_q = 0$ and L_d has the maximum value at this position when injecting the voltage in phase-a. The same principle applies when determining the L_q , with the only difference being, that the area between the north and south poles is aligned with phase-a to determine the q-axis inductance, as illustrated in Figure 5.3.

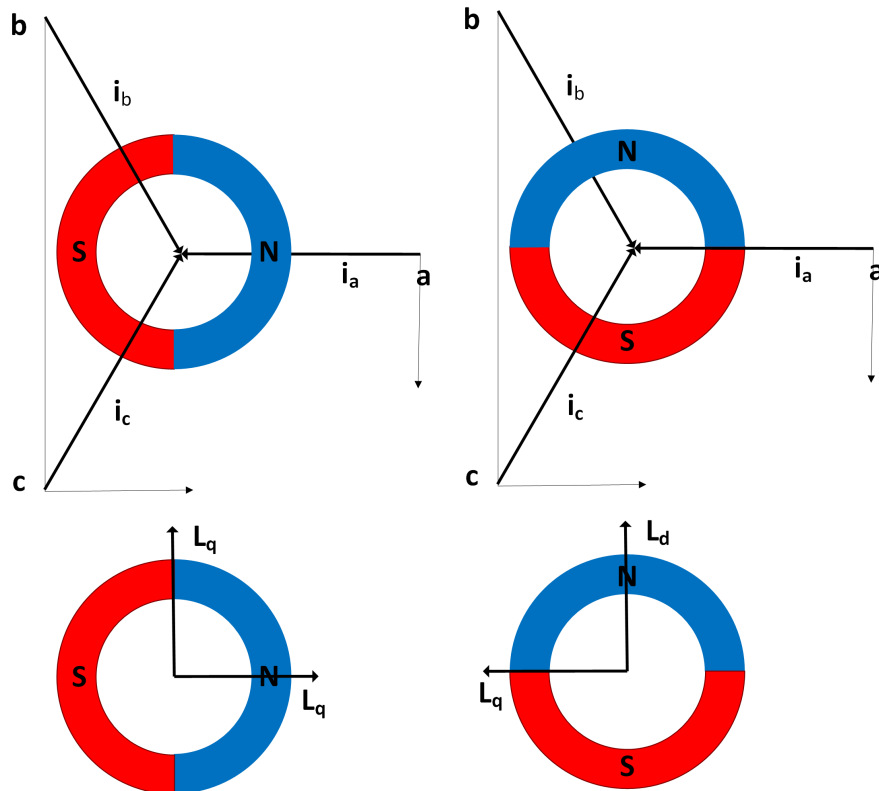


Figure 5.2. Rotor position when de-
termining the d-axis in-

Figure 5.3. Rotor position when de-
termining the q-axis in-

The phase resistance and dq-axis inductance obtained from the motor parameter determination test can be seen in Table 5.1.

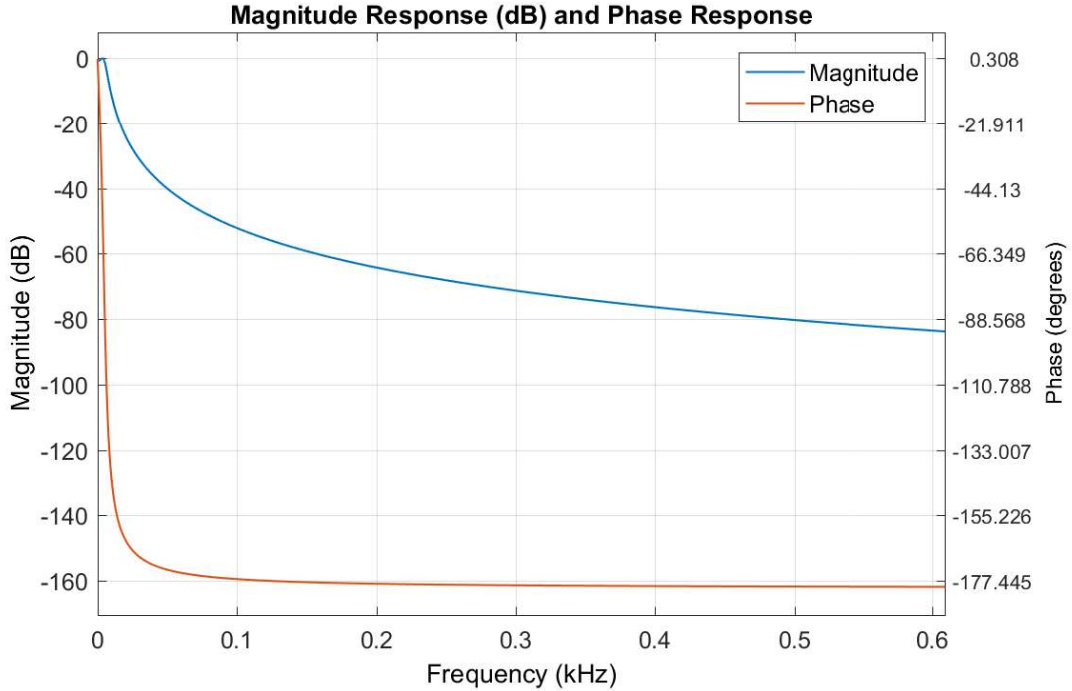
Phase resistance [R]	d-axis inductance [L_d]	q-axis inductance [L_q]
3.03 [Ω]	0.013 [H]	0.016 [H]

Table 5.1. Motor parameters.

5.3 High Frequency Sinusoidal Voltage Injection

In this section, a description will be given on how this high frequency injection method is implemented in the laboratory. More specifically, the considerations and problems in the implementation will be presented. Finally, the obtained results will be presented and analyzed.

Before testing the HF sinusoidal injection a filter needs to be designed, therefore a brief discussion of the chosen filter and parameters will follow. Further discussion of filter design can be found in Appendix B. In this project a sampling frequency of 10 kHz is used therefore the filter must have a high enough throughput. If the position estimation is used in a feedback loop the filter must be stable, for this application no phase shift is desired at the zero and low speed range, therefore the designed filter should consider this. Both filter types have desired characteristics for this project, however because of the sampling frequency the most important feature is the high throughput, therefore a low order IIR filter is implemented. The filter gain and phase response can be seen in Figure 5.4, the designed filter is designed using a cutoff frequency of 5 Hz a sampling of 10 kHz and the Chebyshev 1 method for calculating the coefficients with a maximum order of two.

**Figure 5.4.** IIR filter magnitude and phase response.

5.3.1 Results

In this section the results from the test setup regarding the rotating vector method will be presented. The tests will include a change of frequency and amplitude in order to determine the impact on the position error. All tests are done using electrical degrees. For the first test a frequency of 100 Hz and a voltage amplitude of 20 V is used. The results can be seen in Figure 5.5.

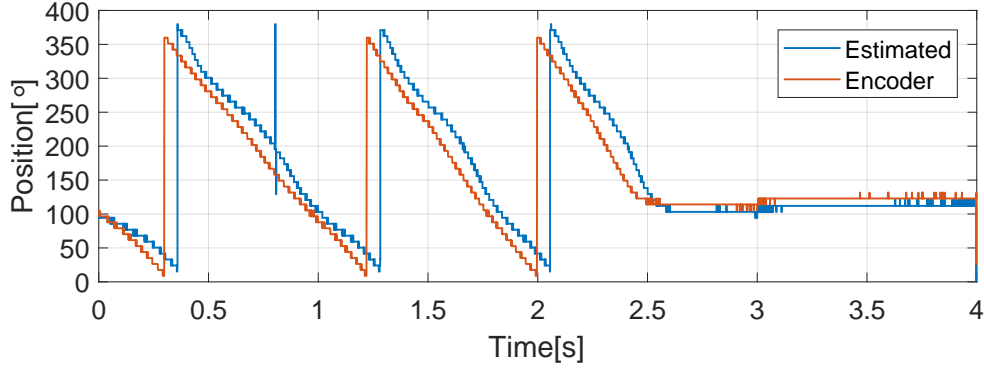


Figure 5.5. Comparison of estimated position with 100 Hz injection and 20 V and encoder.

From the figure it is seen that the error is not constant during the transient states, which could be due to phase shift at low frequencies from the filter which can be seen in Figure 5.4. Once the position reaches steady state the estimation is constant. A calculation of the error revealed an error of 10-30 degrees during transients and 10 degrees at steady state. According to theory an increase in frequency should result in a decrease of the error. In Figure 5.6 and 5.7 a test of 300 and 500 Hz respectively can be seen.

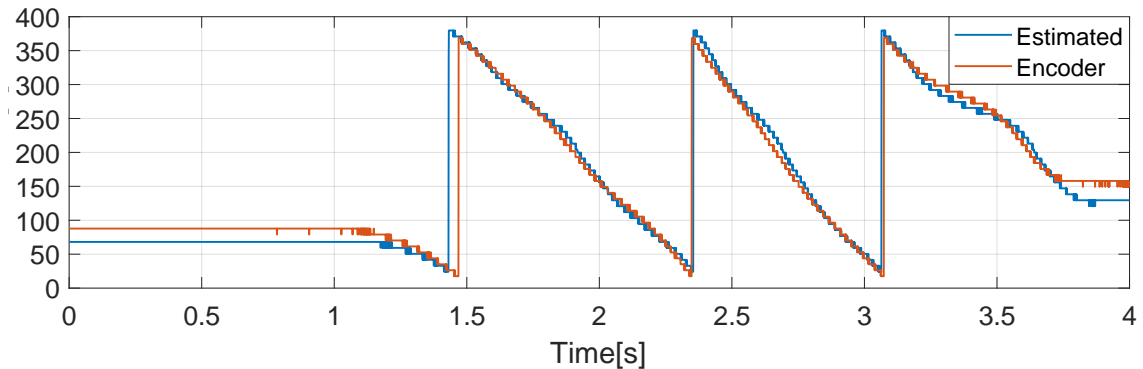


Figure 5.6. Comparison of estimated position with 300 Hz injection and 20 V and encoder.

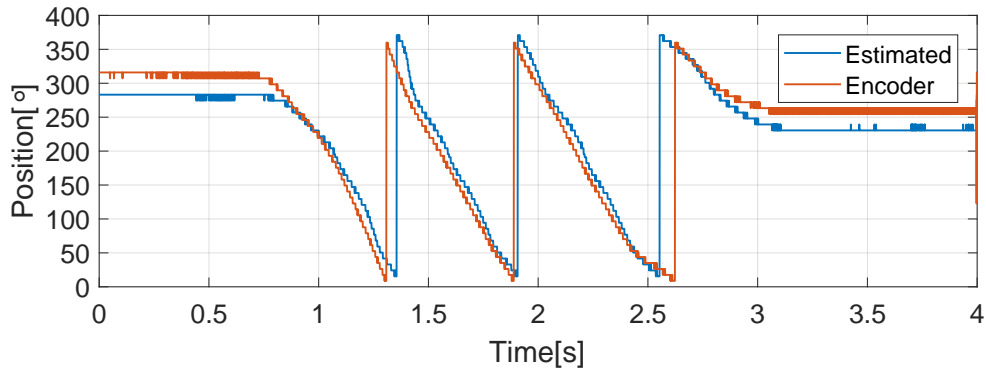


Figure 5.7. Comparison of estimated position with 500 Hz injection and 20 V and encoder.

From the figures it does not seem that the error is reduced at steady state but rather increased. In these tests it can also be clearly seen that the position estimation is influenced by the phase shift of the filter at the transient states. The increased error could be due to the increased reactance of the inductors, resulting in a much lower current, which could be prone to measuring errors from the ADC, if the measuring resistance is not calibrated to the current range. For example, at a voltage amplitude of 20 V and a frequency of 300 Hz the demodulated d-axis current can be calculated from Equation (4.7) and would only be in the range of ± 0.073 A and will decrease even further at higher frequencies and lower voltages. A test was made with a lower voltage input which can be seen in Figure 5.8.

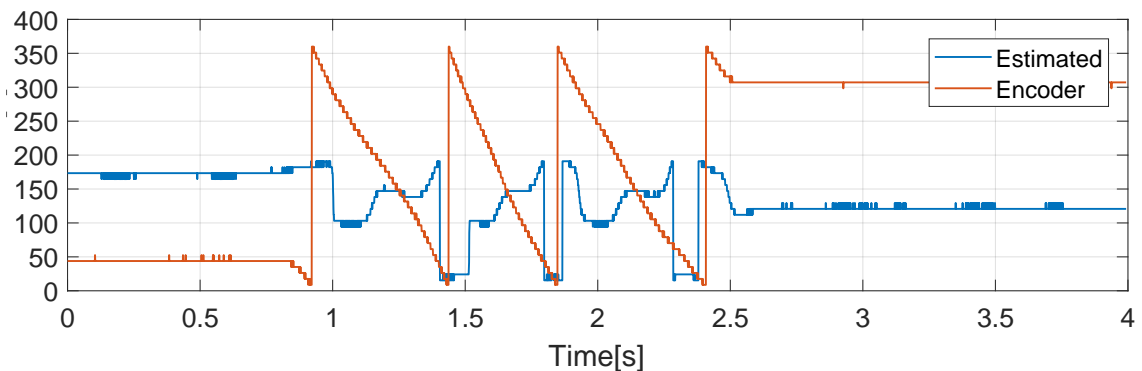


Figure 5.8. Comparison of estimated position with 500 Hz injection and 10 V and encoder.

In the figure it is evident that the current is too small to be measured which can be clearly seen in the estimated position. This is also consistent with the previous discussion. Since a q-axis current will always be present in this method a torque ripple will be introduced to the system, which will decrease with the frequency. This cannot be measured but should be taken into consideration depending on the application.

In this section the high frequency sinusoidal injection method was tested. It was seen that the method was successful at estimating the position of the rotor. From the theory presented in Chapter 4, it was expected that the position estimation would be lower at higher frequencies, this was not the case as the error increased which could be because the current got sensitive to the ADC as it decreased.

Additionally it was seen that the filter had an impact on the estimation during the transient states because of the low cutoff frequency.

5.4 Voltage Pulse Injection

As for the previous high frequency injection method, this section will discuss the implementation of the voltage pulse injection method including the considerations and problems when implementing the method. Furthermore, the obtained results will be presented and discussed.

Unlike the sinusoidal injection method, the voltage pulse injection does not initially need a filter, which made it straight forward in writing the code.

In high frequency injection it is difficult to select a suitable voltage amplitude for the injection. For voltage pulse injection it is known that the current variation is increased when the voltage pulse magnitude is increased. However, an increased voltage pulse magnitude in the q-axis also directly increases the produced torque, as the instantaneous torque is determined as shown in Equation (5.4) for $i_d = 0$.

$$T_e = \frac{3}{2} N_{pp} \lambda_{mpm} i_q \quad (5.4)$$

In Chapter 4 it was assumed that the voltage pulse would not create a rotation of the motor even though the injection was in the q-axis. However, due to the motor in the laboratory having no load it was seen that a low magnitude of the voltage injection created enough torque to rotate the motor. The rotational speed that was created was too high to neglect the back-EMF.

There are a few possibilities to prevent rotation when using voltage pulse injection. A simple solution is to inject the voltage on the estimated d-axis instead of the estimated q-axis. The only difference for the two methods is that the position error will be determined from the imaginary part of the current variation as shown in Equation (5.5) and (5.6).

$$\Delta \bar{i}_{\gamma\delta} = y \Delta t V_m + \Delta y \Delta t V_m (\cos(2\tilde{\theta}_r + 180^\circ) + j \sin(2\tilde{\theta}_r + 180^\circ)) \quad (5.5)$$

$$Im(\Delta \bar{i}_{\gamma\delta}) = \Delta \bar{i}_\delta = \Delta y \Delta t V_m \sin(2\tilde{\theta}_r + 180^\circ) = -\Delta y \Delta t V_m \sin(2\tilde{\theta}_r) \quad (5.6)$$

The position error can be determined and fed to a PLL in the same way as presented in the previous chapter. In applications where there is no need for torque production, it is preferred to inject in the estimated d-axis as torque ripple will be minimized. However, in applications where it is wanted to create torque, as for example in active force feedback, it might be preferred to inject in the estimated q-axis to minimize the losses. This will be explained further in the next chapter.

5.4.1 Results

For the implementation in the laboratory, the voltage pulse was injected in the estimated d-axis in order to minimize the produced torque. In Figure 5.9 the test results of the

position detection is shown. For this test the PLL parameters designed in Chapter 4 are used. The amplitude of the injection voltage is chosen to be 20 V as for the simulations. It can be observed that the estimated position has the ability to follow the measured position from the encoder. However, the estimated position has a lot of noise. This is due to the high parameter values for the PLL, thus the high proportional gain will also amplify the noise which occurs.

The noise can be reduced by either decreasing the PLL parameters or implement a filter on the estimated position. Both of these do however decrease the bandwidth of the system which could become a problem when using a feedback loop for active force feedback. For these tests the rotational speed is low and a decrease in bandwidth is not a problem, it is therefore chosen to decrease the values of the PLL for simplicity.

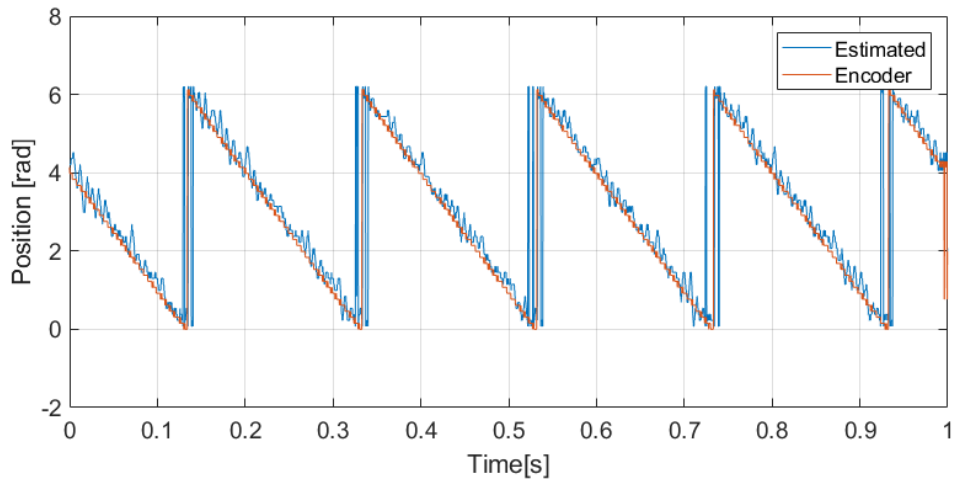


Figure 5.9. Test result of position detection using voltage pulse injection with 20 V magnitude and PLL parameters of $K_p=4269$ and $K_i=9115700$.

In Figure 5.10 the test result of position detection is shown where the PLL parameters are reduced to $K_p = 1000$ and $K_i = 50000$ which are significantly lower than the previous values. Several test were performed with different values and these were concluded to give the optimal performance without the use of a filter. It can be observed that the estimated position follows the encoder position very well with an average error of 8.8° electrical, which corresponds to just under 3° mechanically.

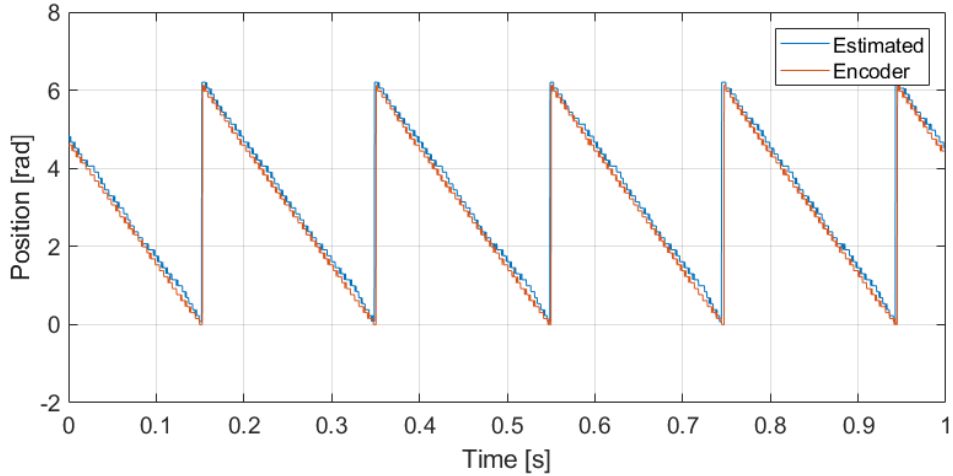


Figure 5.10. Test result of position detection using voltage pulse injection with 20 V amplitude and PLL parameters of $K_p=1000$ and $K_i=50000$.

As it can be observed from the shown results, the voltage pulse injection method has the ability to estimate the position. However, the best results obtained has an average error of 8.8° electrical, which is significantly higher than the position error of 1° obtained from the simulations. This could be due to the back-EMF being neglected and voltage error from the inverter. A simple way to minimize the error is to increase the magnitude of the injected voltage. This will make the voltage error from the back-EMF and the inverter relatively smaller. A higher amplitude of the voltage injection also results in higher current which then can increase the signal to noise ratio [Hechao Wang]. In Figure 5.11 the result of the of the position detection is shown, where the amplitude of the voltage injection is reduced to 10 V instead of 20 V. It can be observed that the estimated position has more error than in the previous test and the average error is increased to 11.6° . It should be noted that the lower voltage amplitude decreases the torque production. The rotational speed is therefore decreased, which also decreases the back-EMF voltage.

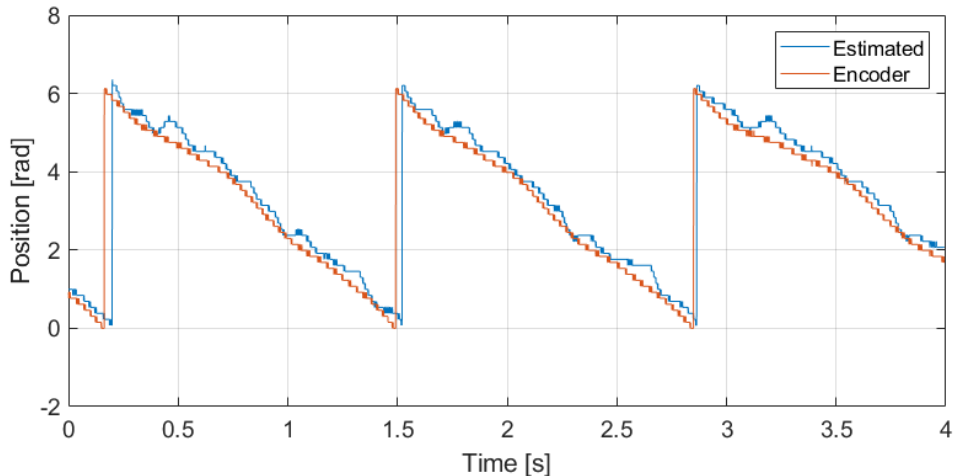


Figure 5.11. Test result of position detection using voltage pulse injection with 10 V amplitude and PLL parameters of $K_p=1000$ and $K_i=50000$.

For all tests that were done, the rotor started rotating even though the voltage was injected in the estimated d-axis. This is another evidence that there is an inverter voltage error, as no torque should be created when the voltage is injected directly on the d-axis. To minimize the voltage error from the inverter, a solution of injecting two voltage pulses in opposite directions has been studied. This method will be discussed in Chapter 8 for further work.

In this chapter the two high frequency injection methods were validated using a laboratory setup for testing. Furthermore, the motor parameters were determined using voltage steps to validate the motor saliency and to compare test result with simulation results. Through experimental work, it was concluded that both the high frequency method and voltage pulse injection had the ability to estimate the position.

For the sinusoidal injection method, it was observed that the results were dependent on the measurement accuracy and that the frequency and voltage injections were limited as a result of this. Furthermore, it was observed that the results were dependent on the designed filter as it could phase shift the estimated position during transient periods making the results more imprecise.

For the voltage pulse injection method, it was initially concluded that an injection in the estimated q-axis produced enough torque to rotate the motor at high speed. It was therefore chosen to inject the voltage in the estimated d-axis to prevent high rotational speed. However, due to inverter voltage error, the voltage injection was not injected directly on the d-axis, which resulted in motor rotation. The rotation was at low speed but still created back-EMF which increased the position error compared to the simulation results. Furthermore, it was observed that when the PLL was designed for a high bandwidth. The PI parameters also amplified the noise in the position estimation, which required that the bandwidth of the PLL was reduced.

For both injection methods it was observed that torque was produced. The sinusoidal injection had a constant torque ripple which was dependent on the frequency and amplitude of the voltage injection. For the voltage pulse method it was observed that torque was produced due to imprecise voltage injection. The torque felt by the user can be reduced by increasing the load of the rotor, which can be a solution for both methods. However, the sinusoidal methods does not have other solutions than to determine the most suited injection frequency and amplitude to minimize the torque, which is felt. On the other hand, the voltage pulse injection method has the opportunity to reduce the inverter voltage error and therefore reduce the torque.

Active Force Feedback

6

In this chapter the principle of active force feedback will be presented. The general idea and purpose of active force feedback will be explained together with the implementation of the method in theory.

A great benefit of using the improved EPS system for steering is the possibility to do active force feedback. Active force feedback has the purpose of enhancing the control of the vehicle when driving as it can return a force to the user when turning the wheel.

A simple way to implement active force feedback is to have a look-up table or function which can determine the needed torque for each position and use it to calculate the needed torque producing current. For this project a simple gain will be used in order to show that when the position changes the torque changes similarly. In real applications it is needed to analyze which exact torque is suitable for each position and for different wheel sizes.

To implement active force feedback in a real application the rotor position is needed to be fed back to the DSP, which then needs to determine the needed current in order to create the suitable torque in the machine. Typically field-oriented control (FOC) is used in order to control the PMSM, due to its decoupled control of torque and flux. With the use of a dq-reference frame, the d-axis current can be placed on the flux axis, which makes it the flux weakening current, and placing the q-axis current orthogonal to the d-axis which makes it the torque producing current [Paul Krause, 2013].

Classically FOC is used as presented in Figure 6.1. FOC consist of two feedback control loops. It can be observed that a rotor speed is fed back and compared with the reference speed in order to determine the rotor speed error. The speed error goes into a speed loop controller, which outputs the needed q-axis current. The d-axis current is as mentioned the flux weakening current and is usually set equal to zero. The currents are compared to the measured dq-axis currents and the error is fed to the current loop controller to determine the voltage, which is fed to the inverter.

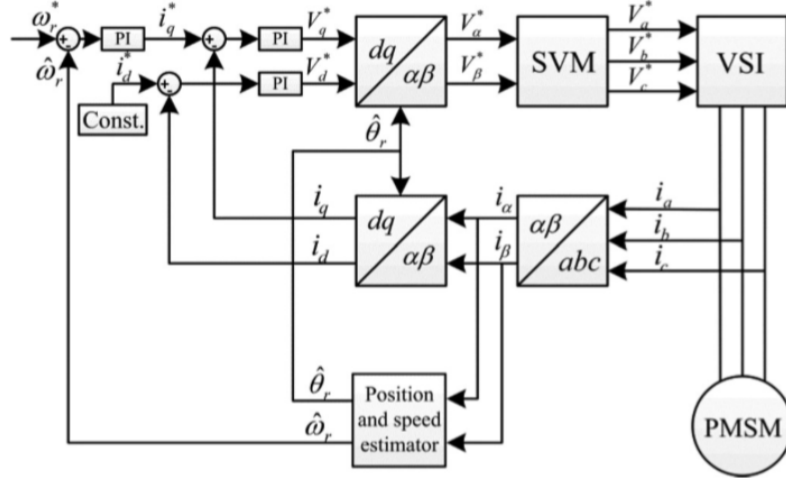


Figure 6.1. Commonly used controller topology for FOC [Ge Xie, 2016].

The control which is needed for active force feedback is very similar to the classical FOC. The difference is that there is no rotor speed reference, and the speed loop is therefore redundant. The position is instead used in order to determine what the torque should be. The overall control diagram can be observed in Figure 6.2. As shown, the force feedback function determines the q-axis current reference from the position, which is estimated using either of the high frequency injection methods. The voltages, which are obtained from the current controller loop are added with the high frequency voltage injection in order to both produce the force feedback torque and also have the needed output signals to determine the rotor position at the same time.

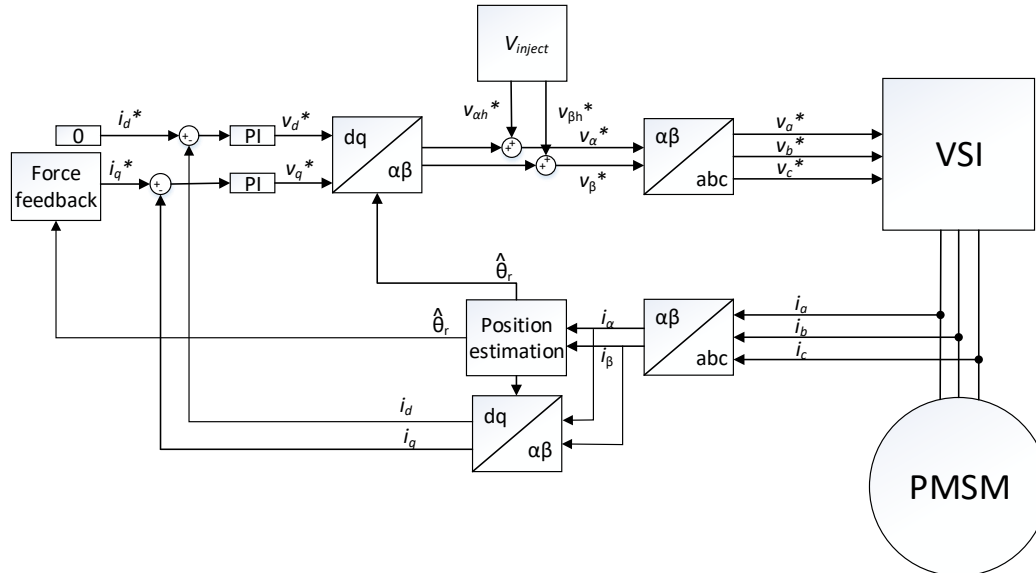


Figure 6.2. Block diagram of force feedback implementation.

6.1 Current Controller Design

As mentioned previously, a current controller loop is needed to supply the motor through the voltage source inverter. For the purpose of active force feedback the controller is required to have a minimal overshoot. This is due to the fact that an overshoot of torque could have severe consequences in a real application, where it could potentially hinder turning the wheel. Furthermore, a fast response is also necessary so that the force, which is felt by the user, is as smooth as possible and not delayed.

The transfer functions can be determined from dq-reference frame machine equation presented in Chapter 3.

$$\bar{v}_{dq} = R\bar{i}_{dq} + \frac{d}{dt}\bar{\lambda}_{dq} + \omega_r \begin{bmatrix} 0 & -1 \\ 1 & 0 \end{bmatrix} \begin{bmatrix} \lambda_d \\ \lambda_q \end{bmatrix} \quad (6.1)$$

Due to the machine still running at low or no speed, the back-EMF term can be seen as disturbance and therefore neglected. This means that the following transfer function can be derived in the Laplace domain as

$$\frac{i_d(s)}{v_d(s)} = \frac{1}{R_s + sL_d} \quad \text{and} \quad \frac{i_q(s)}{v_q(s)} = \frac{1}{R_s + sL_q} \quad (6.2)$$

Due to the digital implementation a delay is needed to be taken into consideration when design the current controller. Typically, the transfer function is as presented in Equation (6.3) [Gene F. Franklin, 2006].

$$G_{delay}(s) = \frac{1}{1.5T_d s + 1} \quad (6.3)$$

where $T_d = 1/10.000$ is the sampling period.

For this project at simple control loop design analysis will be made in order to design suitable PI controllers. The controllers will be determined in the Laplace domain. It should be noted that in this section, the controllers are designed for ideal conditions, where the bandwidth is not decreased due to filters or PLL. As L_d and L_q are different from each other, a PI controller will be designed for each of inductances. The PI controllers will be designed using the method called Modulus Optimum, which has the purpose of cancelling the pole closest to origin and also creating the desired damping factor. The method of designing suitable controller will be presented for the d-axis current. However, the same requirements are applied for both controllers.

Looking at the plant and the delay, the transfer function can be written as

$$G_{delay}(s)G_{plant,d}(s) = \frac{1}{1.5T_d s + 1} \frac{1}{R_s + L} = \frac{1}{1.5T_d s + 1} \frac{1/R}{\frac{L}{R}s + 1} \quad (6.4)$$

Rewriting $\frac{1}{R_s} = K$ and $\frac{L_d}{R_s} = T_p$, the equation can be written as

$$G_{delay}(s)G_{plant,d}(s) = \frac{1}{1.5T_d s + 1} \frac{K}{T_p s + 1} \quad (6.5)$$

It is known that a PI controller can be written as

$$G_c(s) = K_p \frac{T_i s + 1}{T_i s} \quad (6.6)$$

where T_i equals $\frac{K_p}{K_i}$.

As $T_p s + 1 = 0 \Rightarrow s = -\frac{1}{T_p} = -224$, it can be seen that it is the dominating pole, which is wanted to cancel. Therefore, T_i should be equal to T_p . The open loop transfer function for the plant, delay and PI controller therefore becomes

$$G_{dsystem,ol}(s) = K_p \frac{T_p s + 1}{T_p s} \frac{1}{1.5 T_d s + 1} \frac{K}{T_p s + 1} = K_p \frac{1}{T_p s} \frac{1}{1.5 T_d s + 1} K \quad (6.7)$$

This means that the closed loop transfer function becomes a second-order system

$$G_{dsystem,cl}(s) = \frac{K_p K}{1.25 T_{sw} T_p s^2 + T_p s + K_p K} \quad (6.8)$$

It is known that a second order system can be described by its natural frequency, ω_n , and damping factor, ζ

$$G_{2nd}(s) = \frac{\omega_n^2}{s^2 + 2\zeta\omega_n s + \omega_n^2} \quad (6.9)$$

The closed loop transfer function of the system can then be rewritten so that the natural frequency and damping factor can be obtained

$$G_{dsystem,cl}(s) = \frac{\frac{K_p K}{1.5 T_d T_p}}{s^2 + \frac{1}{1.5 T_d} s + \frac{K_p K}{1.5 T_d T_p}} \quad (6.10)$$

As $T_p = \frac{L_d}{R_s}$ and $K = \frac{1}{R_s}$, the transfer function becomes

$$G_{dsystem,cl}(s) = \frac{\frac{K_p}{1.5 T_d L}}{s^2 + \frac{1}{1.5 T_d} s + \frac{K_p}{1.25 T_d L_d}} \quad (6.11)$$

The natural frequency and the damping factor can then be determined as

$$\omega_n = \sqrt{\frac{K_p}{1.5 T_d L_d}} \quad (6.12)$$

$$2\zeta\omega_n = \frac{1}{1.5 T_d} \Rightarrow \zeta = \sqrt{\frac{L_d}{6 T_d K_p}} \quad (6.13)$$

As mentioned in the beginning of this section it is required that the system has a minimum overshoot. This means that the damping factor should be $\zeta = 1$. The proportional term of the controller can therefore be obtained as

$$1 = \sqrt{\frac{L_d}{6 T_d K_p}} \Rightarrow K_{p,d} = 20.7 \quad (6.14)$$

As $T_i = \frac{K_p}{K_i} = T_p = \frac{L_d}{R_s}$. The integral term of the PI controller can be obtained as

$$\frac{K_p}{K_i} = \frac{L_d}{R_s} \Rightarrow K_{i,d} = 4633 \quad (6.15)$$

In Figure 6.3 the step response of the d-axis current control loop is shown. The system has a settling time of 2 ms and an overshoot of 1.5 percent.

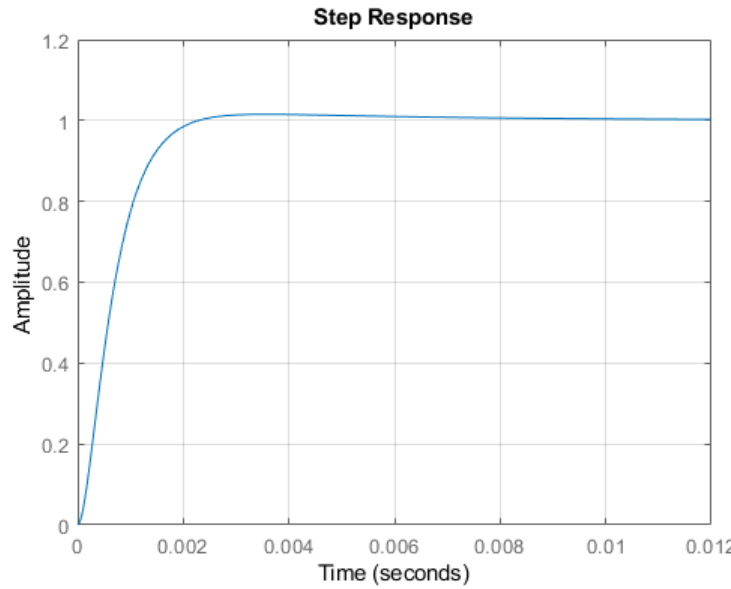


Figure 6.3. Step response of d-axis current controller loop.

The closed loop Bode diagram is shown in Figure 6.4. Analyzing the Bode diagram it can be determined that the magnitude crosses -3 dB at 1750 rad/s, which is where the bandwidth is obtained. This bandwidth corresponds to about 280 Hz, which is significantly lower than 1/10 of the sampling frequency (10 kHz).

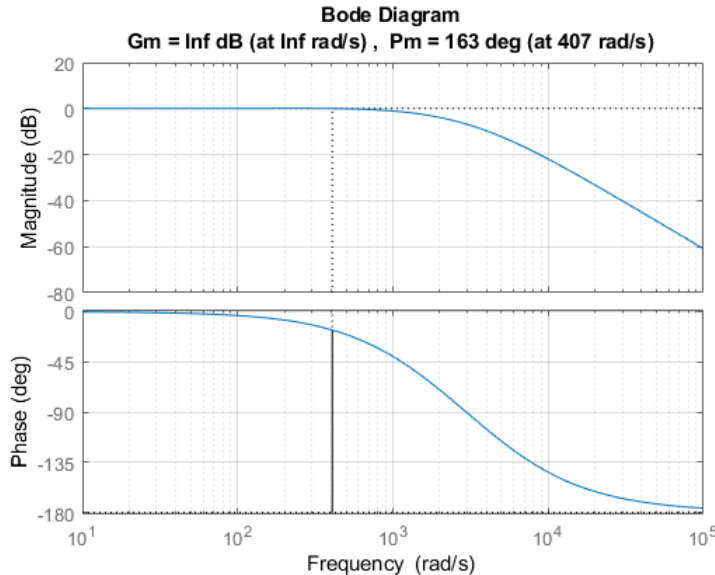


Figure 6.4. Closed loop Bode diagram of d-axis current controller loop.

For the q-axis current the following parameters were obtained using the same method, which gives the same step response and bandwidth.

$$K_{p,q} = 25 \quad \text{and} \quad K_{i,q} = 4633 \quad (6.16)$$

6.2 Implementation of Force Feedback for Sinusoidal Injection

In this section the challenges regarding the implementation of field oriented control when using the rotating vector injection method will be presented.

As mentioned in the previous section, FOC for this application only needs to implement current controllers. Due to the high frequency injection, a lowpass filter on the $\alpha\beta$ -axis currents needs to be implemented in order to control only the fundamental current. A consequence of the low pass filter is reduced bandwidth of the current, meaning a slower response of the PI-controller.

Furthermore, due to the restriction of high throughput from the sampling frequency, the lowpass filter is chosen to have a maximum order of two, thereby decreasing the bandwidth even further, as the cutoff frequency needs to be even lower to attenuate the signal properly. Therefore a higher injection frequency will result in a higher bandwidth as the lowpass filter can achieve a higher cutoff frequency. A demonstration of this effect can be seen in Figure 6.5, where a controller is tuned to a filter with a cutoff frequency of 50 Hz with order two and 600 Hz injection, compared the same controller using a filter designed with a cutoff frequency of 15 Hz. The figures are made using a step of 1 amperes in the q-axis current, $K_p = 1$ and $K_i = 180$.

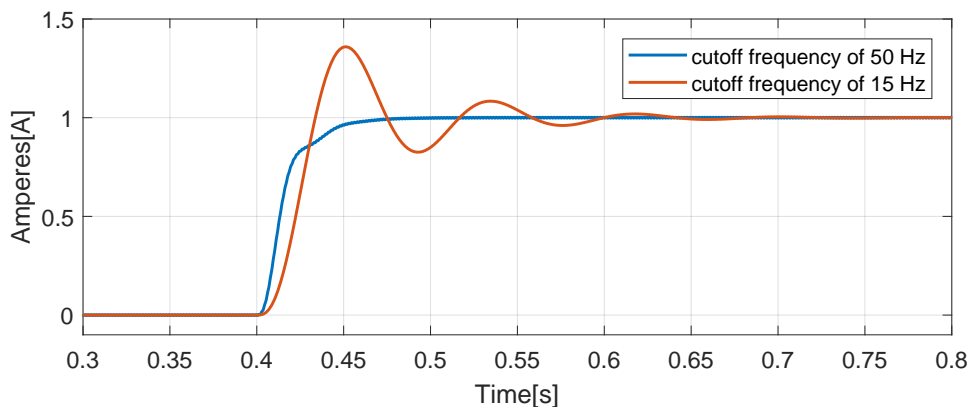


Figure 6.5. Step response of the I_q current using different cutoff frequencies.

From the figure it can be seen that the low cutoff frequency decreases the damping ratio of the step response. Furthermore, the settling time can be seen to be significantly slower than that of the theoretically fastest response of the previous section, which is also evident when looking at the controller parameters.

The lowpass filter has a great influence on the bandwidth of current loop, which results in a slower controller. However, for this application only low or no speed is considered therefore the controller is not required to track high velocity changes and could still be suitable. In Figure 6.6 a current reference reverse proportional to the estimated position is seen with the output torque.

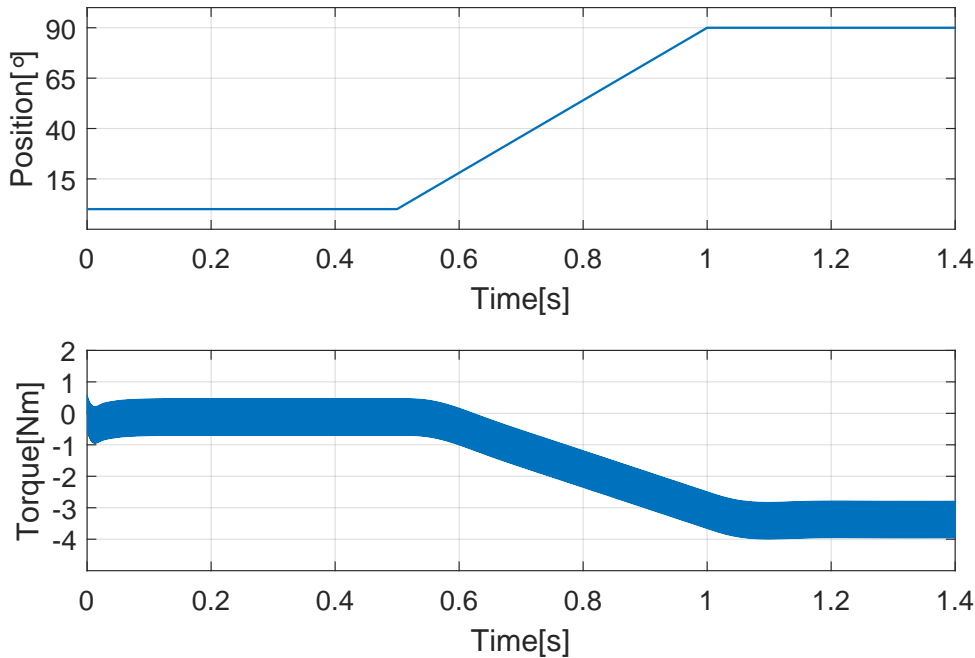


Figure 6.6. Top position of rotor Bottom torque produced.

In the figure it can be seen that the torque is inverse proportional to the position as was desired. A fundamental torque is seen with a torque ripple from the HF injection, a small delay can be seen between the settling times of the position and torque, this could be due to the low bandwidth of the PI controller.

6.3 Implementation of Force Feedback for Voltage Pulse Injection

In this section the implementation of force feedback for voltage pulse injection will be presented. The section will contain an explanation of how to implement the force feedback loop and its challenges.

A great benefit of the voltage pulse injection is that a voltage pulse is given over every switching period. The other switching period can then be used for force feedback injection. This means that it is not needed to add two different voltage injections and then decoupling them again.

As briefly mentioned in Chapter 5, it is preferred to inject the voltage in the estimated d-axis if it is desired to produce no torque. The whole purpose of force feedback is to produce torque, and it is therefore preferred to inject in the estimated q-axis. This means that instead of only producing torque every other switching period, the injection voltage for position detection can contribute in generating torque. This will both reduce the power loss and also give a more constant and therefore smooth torque production.

Compared to sinusoidal injection, the voltage pulse injection can directly give the $\alpha\beta$ -axis currents without the need of a filter. Although it was determined from the laboratory

tests that the PI parameters for the PLL had to be reduced it does not impact the current controller, as the change in rotor position is minimal at low speed. This means that the bandwidth for the current is not reduced and the two designed current controllers can be implemented.

In Figure 6.7 the Simulink result of the torque production is shown during a ramp going from 0° to 90° . It can be observed that the torque follows the position in the opposite direction as it should. As for the sinusoidal injection, a delay and torque ripple do occur. However, it can be observed that the delay is significantly lower due to the higher bandwidth of the current controller. Furthermore, as the voltage is always injected in the estimated q-axis, the torque ripple is lower than for the sinusoidal injection method.

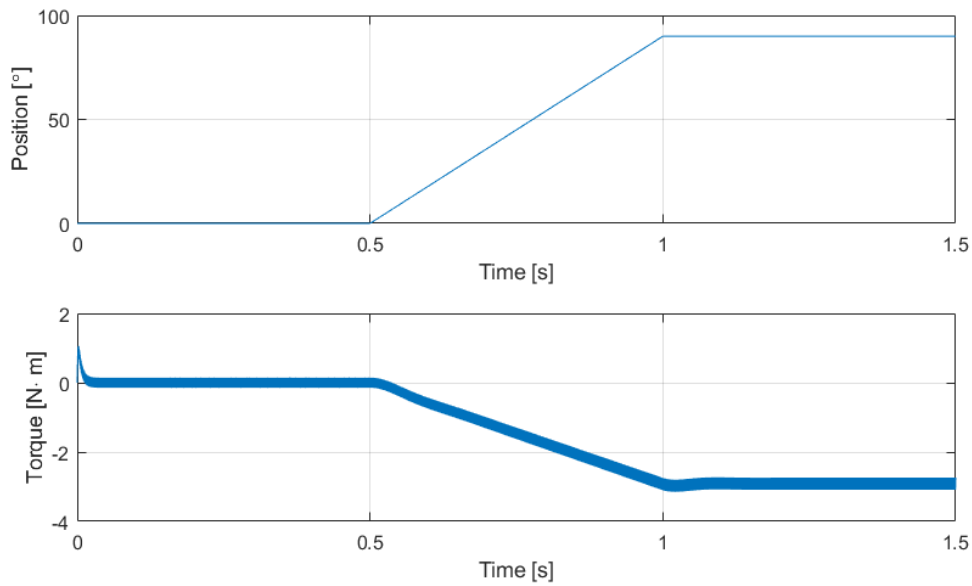


Figure 6.7. Simulink result of torque production during a 90° ramp. Top picture shows rotor position and bottom picture shows torque produced

In this chapter purpose of active force feedback was explain. FOC was chosen to be used for the current control loop and was therefore investigated.

Additionally, two current controllers were designed using Modulus Optimum in order to have a current response which was both fast and had no overshoot. Active force feedback was then implemented in Simulink for both the HF injection methods. For the sinusoidal injection method it was found that an additional filter was needed to determine the fundamental current for the current controller feedback. As a result of this, the bandwidth of the current controllers had to be reduced. The sinusoidal injection method could nonetheless still produce the desired torque compared to the rotor position. However, due to the low bandwidth of the current controllers a delay was observed. Furthermore, a torque ripple was present from the HF injection. For the voltage pulse method the designed current controller could be used as the fundamental currents could be measured directly with a ripple due to the injection. As the voltage was injected in the estimated q-axis for both switching period, it was observed that this HF injection method could produce the desired torque with less delay and torque ripple than the sinusoidal method.

Conclusion

7

In the introduction electric vehicles were the main focus. More specifically the electronic power steering system. The current power steering system was compromised of an encoder and torque transducer attached to the steering column which connects to a computational unit, in order to control the position of the wheels. An alternative system was proposed where the steering column is replaced with a permanent magnet machine, which using certain voltage injection techniques could detect the position. This system would have the advantage of removing the steering column in order to release space in the cabin for the driver on off-highway vehicles to achieve a better view and ergonomic seating. Additionally the use of a permanent magnet motor introduces the possibility of feedback control meaning the torque can be controlled to achieve full control of the sensitivity of the steering.

Based on the application it was concluded that the position detection techniques should operate under no or low speed conditions. The chosen techniques should therefore accommodate this criteria. A brief study of several techniques revealed that the back-EMF based position detection is only useful at high speed applications, whereas a high frequency sinusoidal and voltage pulse injection methods proved promising as they used the saliency of the machine to detect the position, which does not require high rotational speed.

In order to derive the expressions used to determine the position in the respective methods, a high frequency low speed model in the estimated frame of the permanent magnet machine is necessary. During the derivation of this model, it was assumed the resistance was negligible due to the high frequency, and the back-EMF as well due to the low speed aspect. Due to the introduction of the estimated reference frame the high frequency low speed machine model proved to have a current term related to the position.

With the proper machine model in place, the high frequency sinusoidal injection method was tested. In this method a high frequency sine and cosine was injected in the $\alpha\beta$ -reference frame, respectively. By doing so it was seen that projecting the output currents to the dq-frame using the theta from the injection, resulted in a expressing containing a term directly position of the rotor. To extract the position information, a filter was implemented in order to demodulate the higher unwanted frequencies. A model was built and tested in Simulink, where it was proven that the phase resistance still had a influence on the accuracy of the position estimation, as it was seen that a lower resistance resulted in a lower estimation error. Therefore, it was tested if a higher frequency injection resulted in a better estimation, which proved to be correct. By using a trigonometric relation, it was seen that a filter-less estimation of the position was achievable. This method proved to result in higher estimation errors and it was therefore chosen not to test this further.

In the voltage pulse injection method, a voltage command injected directly on the estimated q-axis was performed. This method utilizes the pulse injection to create a current difference, which projected to the dq-frame using the estimated position, could estimate the position by feeding the real part to a phase-locked loop. The phase-locked loop was tuned to the theoretically best performing parameters, in order to achieve the optimal response for the estimated position. A model was built and tested in Simulink, which proved that the method was suitable to detect the position, and actually achieve zero steady state error, but had a small error during the transient states.

With the concept proved for both methods, they had to be tested in the drives laboratory. The sinusoidal injection method was tested using different frequencies in order to test whether theory was in accordance to practice. It was seen that at a injection of 100 Hz and 20 V the estimated error was 10 electrical degrees at steady state, and varying error during transient response due to the low order filter implemented. When increasing the frequency, the error was seen to increase at steady state, which was thought to be because of the low current produced as a result of the reactance. Therefore a test was made with a lower voltage which produced unsatisfactory results, where the estimated position was not found, which was concluded to be caused by the low current.

When testing the voltage injection method, it was decided to test different control parameters for the phase locked loop in order to determine the effect on the position estimation, and inject the voltage in the d-axis instead in order to produce zero torque. The designed parameters were tested first which were tuned to achieve the best possible response. It was seen that the noise was amplified too much rendering the output useless. The bandwidth of the PI controller of the phase locked loop was therefore reduced which produced a much better result. Unfortunately, due to the voltage error from the inverter, it was not possible to inject the voltage directly on the d-axis, which resulted in a rotation of the motor, and an error of approximately 8.5 electrical degrees compared to the 1 degree of the simulation.

As mentioned in the introduction, force feedback could achieve desirable characteristics such as full control of the sensitivity. It was therefore investigated how this could be achieved. For both methods it was chosen to implement field-oriented control. As the position will be the reference, only the current loop is needed. In sinusoidal injection, a low pass filter on the dq-axis current is necessary as only the fundamental current is desired for the control of the torque. Due to the low pass filter, a lower bandwidth of the system is introduced, which will affect the response of the PI controller. However, as this application is only low speed, the low bandwidth proved sufficient in order to generate the desired torque with a small delay, which contained a fundamental torque and ripple from the high frequency injection.

In order to implement force feedback in the voltage pulse injection, two sections were defined, one where the voltage for the field oriented control is calculated, and one where the injection voltage is calculated. As no filter is implemented in this method, the bandwidth was not affected, therefore the torque response had almost no delay, and a smaller torque ripple due to the voltage pulse injection.

To conclude on the main objectives of this report which was to test two different position estimation methods based on the saliency of the motor, and test which one was the most suited for low speed applications. The sinusoidal injection proved to be able to estimate the position, where the precision was dependent on the motor phase resistance, the filter and the injection frequency. For active force feedback, field-oriented control was a successful method which could achieve the desired output torque, despite a low bandwidth from the filter. From the tests in the laboratory it can be concluded that to achieve a good position estimation the phase resistance should be low, and the frequency should be as high as possible without compromising the measuring accuracy.

The voltage pulse injection method proved to be able to detect the position of the machine with zero steady state error in the simulation, with only the PI parameters affecting the position estimation. For active force feedback, field oriented control was a successful method which could achieve the desired output torque. From the tests in the laboratory it was evident that due to the voltage errors it was not able to inject the voltage directly in the estimated d-axis, causing a higher estimation error and rotation of the machine. This method proved to be more reliable than the sinusoidal injection, but the inverter voltage error needs to be compensated for in order to work properly.

Further work 8

This chapter will propose suggestions for topics of interest with respect to further work outside the scope of this project. The scope of this project was limited to the investigation and implementation of different sensorless position estimation methods, thereby making it rather theoretical. It could therefore be interesting to expand the scope and take a more practical approach.

8.1 Improvement of Measurement Accuracy

Since both sensorless position detection methods require accurate current measurement in order to determine the position of the rotor within an acceptable error margin. Therefore it would be interesting to investigate the current measurements going through the measurements box width respect to amplitude and resolution. The measuring box used for this project was made out of current transducers (LEM modules) rated at a maximum input of 70 A and had conversion ratio of (1:1000). This gives an low output current since sensorless position estimation does not produce such high current, especially not when injecting at high frequency as the current is inverse proportional to the frequency when having a fixed voltage. Having low current amplitude as an output could give increased error, since small accuracy error from the LEM module has a greater impact on low output amplitude. Choosing or modifying the measurement box to have a lower conversion ratio could therefore be preferable.

Besides the amplitude of the current output it could be interesting to investigate possible methods of increasing the resolution of the ADC. The ADC has an operating range at 3.3 V and a corresponding 12-bit resolution. In order to get the maximum resolution it is important to utilize the full operating range. The voltage input to the ADC is determined either by the measuring resistance located at the ADC input terminal on the ancillary circuit or by the current output of the measuring box. Investigating the current amplitudes of the sensorless position estimation methods, would give a good foundation to choose a suitable measuring resistance or change the conversion ratio om the measuring box, as a high current low resistance combination could lead to unwanted voltage errors, which makes it difficult to control the operating range of the ADC.

8.2 Digital Filter Design

Another parameter that has an influence on the accuracy of the position detection methods is the filters ability to remove noise, since high amount of noise would give a position error. Increasing the order of the filter would give a better attenuation since the transition band

decreases when the order increases. However, having a filter of higher order would result in higher computational time, which would limit the sampling frequency and thereby slowing down the overall system response. Several things could be investigated in order to either increase the response of the system or the accuracy of the measurement.

Optimizing the c-code could be a way of reducing the overall computational time, thereby allowing additional time for the filter to process the signal.

8.3 Minimize Inverter Voltage Error

As mentioned in Chapter 5, there are several factors that can result in less accuracy of the voltage pulse injection method. One of the factors that was observed in this project was the effect of inverter voltage error. It was observed that the voltage was not injected directly at the estimated position. A solution to this problem is to inject two opposite voltage vectors. In Chapter 4 the voltage pulse method presented had a voltage injected in either the q- or the d-axis for one switching period and then injecting nothing in the other period, which then can be used to inject the voltage needed for FOC as mentioned in Chapter 6. The injection scheme is shown in Figure 8.1. For the double pulse method one switching period is kept for FOC but instead of having one period for injection, two will be used with opposite voltage injections as shown in Figure 8.2.

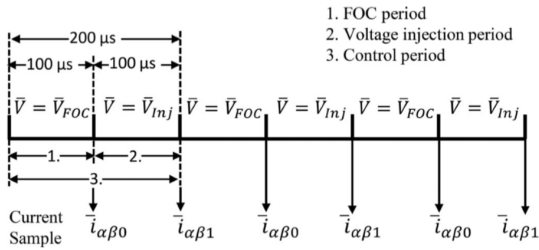


Figure 8.1. Single voltage injection scheme [Ge Xie, 2016].

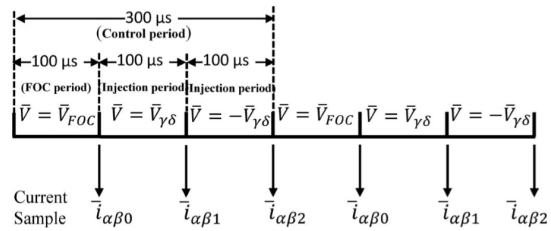


Figure 8.2. Double voltage injection scheme [Ge Xie, 2016].

For the double pulse injection method, the voltage can be injected in the estimated q-axis in the first injection period as shown in Equation (8.1) and then in the opposite direction in the next as shown in Equation (8.2). It is assumed that the inverter voltage error is constant during the two switching periods.

$$V_m e^{j\theta_{v1}} \approx V_m e^{j90^\circ} - \Delta \bar{v}_{inv} \quad (8.1)$$

$$V_m e^{j\theta_{v2}} \approx V_m e^{-j90^\circ} - \Delta \bar{v}_{inv} \quad (8.2)$$

By measuring the current before and after each of the injection periods the current differences can be calculated and transformed to the estimated dq-reference frame which gives the following current variations

$$\Delta \bar{i}_{\gamma\delta 1} = \left(y + \Delta y \cdot e^{j2(\bar{\theta}_r - 90^\circ)} \right) \cdot \Delta t (V_m \cdot e^{j90^\circ} - \Delta \bar{v}_{inv}) \quad (8.3)$$

$$\Delta \bar{i}_{\gamma\delta 2} = \left(y + \Delta y \cdot e^{j2(\bar{\theta}_r + 90^\circ)} \right) \cdot \Delta t (V_m \cdot e^{-j90^\circ} - \Delta \bar{v}_{inv}) \quad (8.4)$$

As for single voltage pulse injection, the real part of the current variations contain the position error, and for the double pulse it is possible to subtract the two real part, which then makes it possible to neglect the inverter voltage error as shown in the following equations [Ge Xie, 2016]

$$\begin{aligned} \operatorname{Re}(\Delta\bar{i}_{\gamma\delta 1} - \Delta\bar{i}_{\gamma\delta 2}) &= -\Delta y \Delta t V_m \sin(2\tilde{\theta}_r - 180^\circ) - y \Delta t \Delta \bar{v}_{inv} \\ &\quad - \Delta y \Delta t V_m \sin(2\tilde{\theta}_r + 180^\circ) + y \Delta t \Delta \bar{v}_{inv} \\ &= 2\Delta y \Delta t V_m \sin(2\tilde{\theta}_r) \end{aligned} \quad (8.5)$$

8.4 Reduction of Acoustic Noise

Besides the theoretically aspect of implementing sensorless position estimation, there is also a concern regarding the environmental health as acoustic noise can occur within the range of 20 Hz - 20 kHz due to switching.

For this project, two position estimation methods were investigated. For the sinusoidal voltage injection, different frequencies of 100 Hz, 300 Hz and 500 Hz were implemented and tested. These frequencies all lies within the acoustic audible range and may be desirable to increase or decrease with respect to the environmental health. However, this also depends upon the intensity of the frequency, as lower frequencies requires higher intensity in order to be noticeable.

For voltage pulse injection, a switching frequency of 10 kHz was used. The chosen frequency did produce noticeable acoustic noise in the laboratory. By increasing the switching frequency to at least 20 kHz, the noise will become ultra sound which can not be heard by humans. This does however decrease the measured current variation as it is dependent on the time from one sampling to the next. Furthermore, it increases the requirement for the c-code and DSP, as the maximum allowed computational time is more than halved.

8.5 Implementation of Active Force Feedback

In Chapter 6 active force feedback was investigated and implemented in theory. It could therefore be of interest to implement force feedback in the laboratory to validate the theory. In order to implement force feedback in the laboratory, it is first needed to test and tune the current controllers. This is done by giving a current reference and analyzing the measured current response. It is then possible to implement the rotor position feedback to determine the real reference current which is fed to the current controller loop. The final test would then be to determine suitable torque compared to the different rotor positions.

Bibliography

Emmanuel C. Ifeachor, 2002. Barrie W. Jervis Emmanuel C. Ifeachor. *Digital Signal Processing A Practical Approach*. ISBN: 0201-59619-9, Handbook. Pearson Educated Limited, 2002.

Ge Xie, 2016. Member IEEE Sanjeet Kumar Dwivedi Senior Member IEEE Jesper Riber Rosholt Frede Blaabjerg Fellow IEEE Ge Xie, Kaiyuan Lu. *Minimum-Voltage Vector Injection Method for Sensorless Control of PMSM for Low-Speed Operations*, 2016.

Gene F. Franklin, 2006. Abbas Emami-Naeini Gene F. Franklin, J. David Powell. *Feedback Control of Dynamic Systems*. ISBN:0-13-149930-0, Handbook. Pearson, 2006.

Hechao Wang. Dong Wang Frede Blaabjerg Hechao Wang, Kaiyuan Lu. *Investigation of Various Position Estimation Accuracy Issues in Pulse-Injection-based Sensorless Drives*.

J.-L. Chen, 2009. C.-L. Chen J.-L. Chen, T.-H. Liu. *Design and implementation of a novel high-performance sensorless control system of interior permanent magnet synchronous motors*, 2009.

Paul Krause, 2013. Scott Sudhoff Steven Pekarek Paul Krause, Oleg Wasynczuk. *Analysis of Electric Machinery and Drive Systems*. ISBN:978-1-118-02420-4, Handbook. John Wiley & Sons, 2013.

Sungmin Kim. Seung-Ki Sul Sungmin Kim. *Sensorless Control of AC Motor - Where are we now?*

Analog to Digital Conversion A

In this chapter the principle of digital to analog conversion and vice versa will be presented. The importance of correct conversion will be explained and the factors causing potential errors will be stated.

In order to implement sensorless control, it is necessary to read analog signals such as the current from the motor and discretize it in order to interact with the algorithm used to determine the position.

Performing AD conversion is rather simple and can be done knowing the bit resolution and the reference voltage of the ADC. The resolution for the ADC used in this project is 12-bit and the reference voltage is 5 V.

Equation A.1 and A.2 respectively states the conversion ratio, going from analog to digital and vice versa, where n is the bit resolution of the converter and K is a gain.

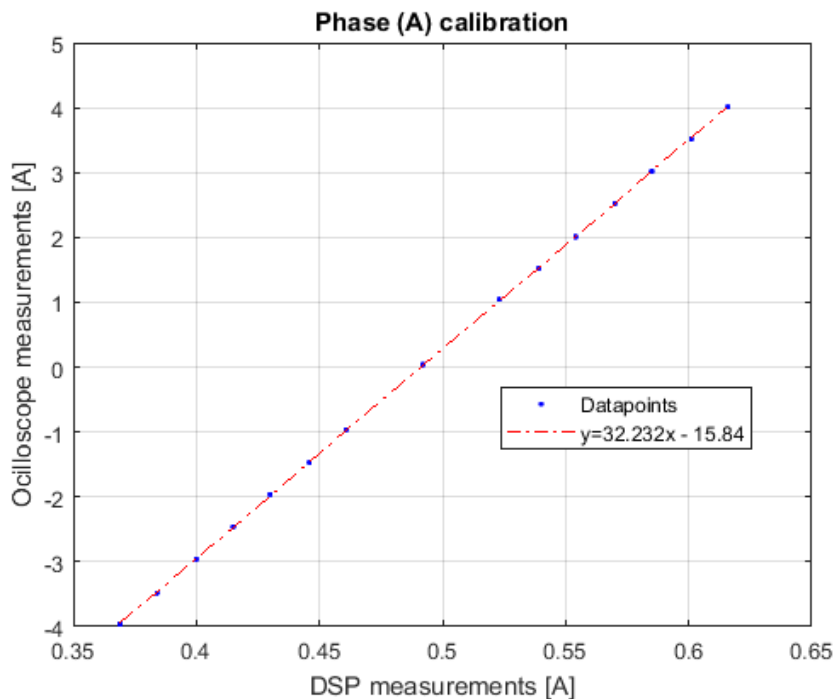
$$ADC_{meas} = 2^n \cdot \frac{V_{in}}{V_{ref} \cdot K} \quad (\text{A.1})$$

$$DAC_{meas} = \frac{ADC}{2^n} \cdot V_{ref} \cdot K \quad (\text{A.2})$$

In order to minimize potential position error caused by wrong measurements, it is necessary to do a calibration of the DAC. This is done by measuring the current of each phase going into the motor using current probes and a oscilloscope to display the measurements. These measurement are then used together with the measurements from the ADC, obtained simultaneously with the probe measurements, to obtain a gain and offset, thereby relating the probe readings with the ADC readings. This relation can then be used to calibrate the DAC output of the DSP.

The measured values for all three phases can be seen in Table A.1 followed by the gain and offset values obtained for each phase illustrated in Figure A.1, A.2 and A.3.

Current input	DSP1(A)	DSP2(B)	DSP3(C)	Scope(A)	Scope(B)	Scope(C)
-4,0	0,369	0,372	0,371	-3,96	-3,96	-3,96
-3,5	0,384	0,387	0,387	-3,48	-3,48	-3,48
-3,0	0,4	0,403	0,402	-2,96	-2,96	-2,96
-2,5	0,415	0,418	0,418	-2,46	-2,47	-2,46
-2,0	0,43	0,433	0,433	-1,96	-1,96	-1,96
-1,5	0,446	0,449	0,449	-1,47	-1,46	-1,45
-1,0	0,461	0,465	0,464	-0,96	-0,96	-0,96
0,0	0,492	0,495	0,495	0,04	0,04	0,04
1,0	0,523	0,527	0,526	1,04	1,04	1,05
1,5	0,539	0,542	0,542	1,52	1,52	1,52
2,0	0,554	0,558	0,557	2,01	2,02	2,04
2,5	0,57	0,573	0,573	2,52	2,52	2,52
3,0	0,585	0,588	0,588	3,02	3,02	3,03
3,5	0,601	0,603	0,604	3,52	3,52	3,52
4,0	0,616	0,618	0,619	4,01	4,02	4,01

Table A.1. DAC Calibration using DSP and Oscilloscope.**Figure A.1.** Calibration of phase a current using linear regression to fit DSP measurement with current probe measurement.

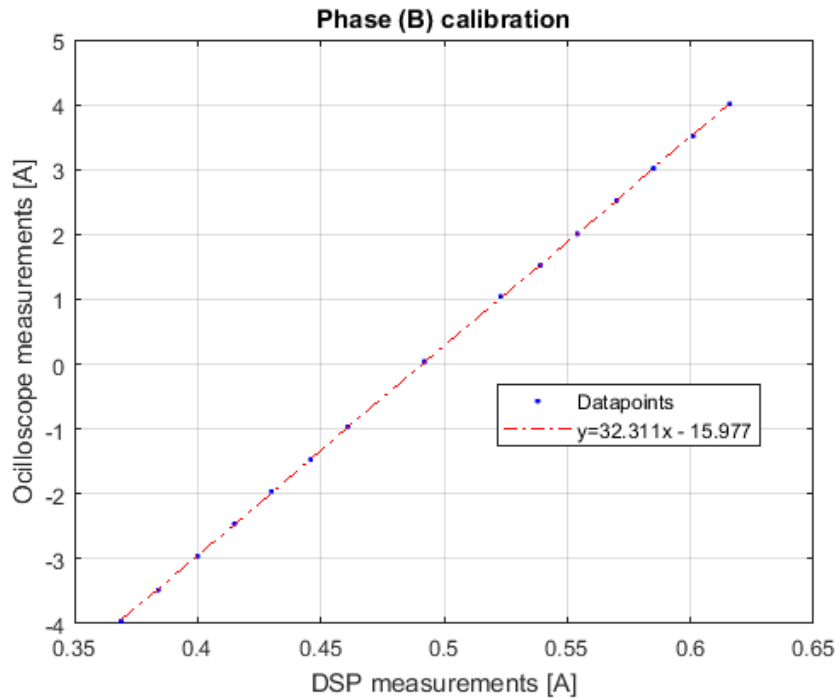


Figure A.2. Calibration of phase b current using linear regression to fit DSP measurement with current probe measurement.

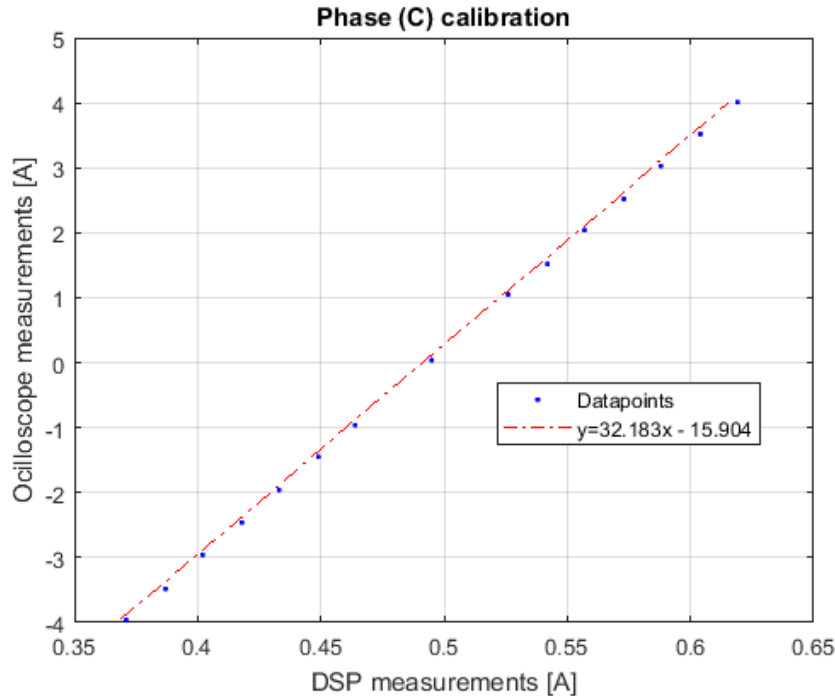


Figure A.3. Calibration of phase c current using linear regression to fit DSP measurement with current probe measurement.

Digital Filter Implementation B

As mentioned in the sinusoidal injection method in Chapter 4, a filter is needed. Therefore, this section will give a description of digital filters, and the choices made regarding the implemented filter will be discussed.

Digital filters can be divided into two categories the finite impulse response(FIR) or the infinite impulse response(IIR). The filters response can be characterized by their respective transfer functions. The FIR transfer function is seen in Equation (B.1) and IIR in Equation (B.2). As infinite response would not be feasible, the IIR filter has been written in its recursive form.

$$H(z) = \sum_{k=0}^{N-1} h(k)z^{-k} \quad (\text{B.1})$$

$$H(z) = \sum_{k=0}^N b(k)z^{-k} / \left(1 + \sum_{k=1}^M a(k)z^{-k} \right) \quad (\text{B.2})$$

When realizing the FIR filter, it can be directly implemented using Equation (B.1) as shown in Equation (B.3).

$$y(n) = \sum_{k=0}^{N-1} h(k)x(n - k) \quad (\text{B.3})$$

where $x(n-k)$ is the input and $h(k)$ is the coefficient. From the equation it can be observed that in order to get one output from the filter, it is necessary to make $N-1$ sums and store $N-1$ inputs. As a consequence of this, the implementation of a FIR filter can have low throughput if the number of coefficients is high.

To realize the IIR filter in the direct form from Equation (B.2), the filter is often converted to cascaded second order sections, as for higher order filter it becomes very sensitive to finite wordlength effects. The second order cascaded IIR filter is realized using the canonical form of the second order sections, characterized by the following equations.

$$H(z) = \prod_{k=0}^{N/2} \left[\frac{b_{0k} + b_{1k}z^{-1} + b_{2k}z^{-2}}{1 + a_{1k}z^{-1} + a_{2k}z^{-2}} \right] \quad (\text{B.4})$$

$$w_k(n) = x(n) - a_{1k}w(n - 1) - a_{2k}w(n - 2)$$

$$y_k(n) = b_{0k}w_k + b_{1k}w(n - 1) + b_{2k}w(n - 2)$$

Where $x(n)$ is the input, $w(n)$ is an internal node of the output, $y(n)$ is the output of each section feeding the next, meaning the input to $w_2(n)$ will not be $x(n)$ but $y_1(n)$, a block diagram representation can be seen in Figure B.1.

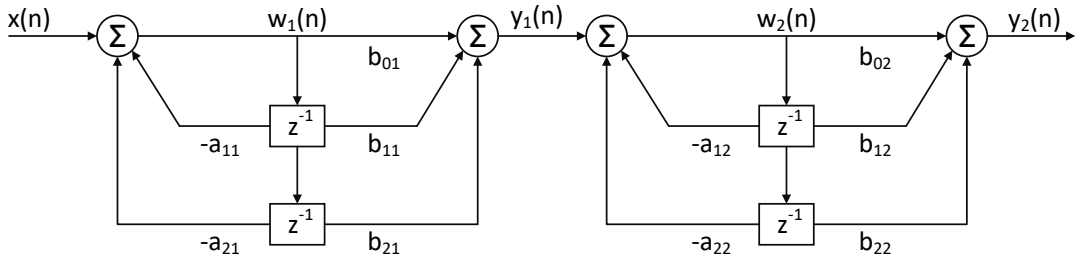


Figure B.1. Second order cascaded IIR filter using canonical form.

From the equation it can be seen that, only second order delays are needed and therefore it is only necessary to store two previous inputs. And as IIR filters will give fewer coefficients than FIR filters, it can produce higher throughput, since fewer calculation are needed. Besides the throughput, another difference between FIR and IIR filters are the phase shift of the response. FIR filter can have linear phase shift, meaning no phase distortion is introduced, whereas the IIR filters has non linear phase shift especially at the band edges. Additionally FIR filters are always stable, which can not always be guaranteed with IIR filters. When choosing between IIR and FIR filters the application has to be taken into consideration in order to determine the best suited filter.[Emmanuel C. Ifeachor, 2002]